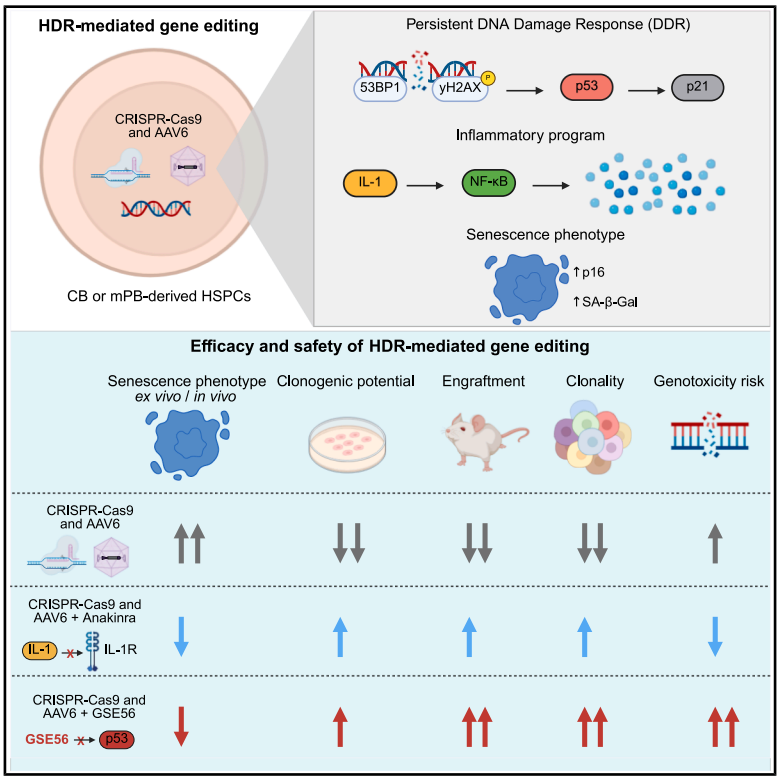
Cell Reports
Medicine

Article

Senescence and inflammation are unintended adverse consequences of CRISPR-Cas9/AAV6-mediated gene editing in hematopoietic stem cells

Graphical abstract



Highlights

- CRISPR-Cas9/AAV6 gene editing elicits senescence and inflammatory programs
- HDR-edited HSPCs display the highest accumulation of senescence markers
- Senescence mitigation enhances polyclonal long-term hematopoietic reconstitution
- Anakinra treatment reduces the genotoxicity risk associated with gene editing

Authors

Anastasia Conti, Kety Giannetti, Federico Midena, ..., Toni Cathomen, Luigi Naldini, Raffaella Di Micco

Correspondence

dimicco.raffaella@hsr.it

In brief

HDR-mediated long-range gene editing in human HSPCs remains challenging. Conti et al. reveal that CRISPR-Cas9/AAV6 HDR editing induces a senescence-like state, impairing HSPC functionality post-transplant. Anakinra, an IL-1 antagonist, mitigates senescence, enhances polyclonal hematopoietic reconstitution, and reduces genotoxicity risk, providing a framework for more effective and safer HSPC-based therapies.

Conti et al., 2025, Cell Reports Medicine 6, 102157
June 17, 2025 © 2025 The Author(s). Published by Elsevier Inc.
https://doi.org/10.1016/j.xcrm.2025.102157

CellPress

Cell Reports Medicine

CellPress
OPEN ACCESS

Article

Senescence and inflammation are unintended adverse consequences of CRISPR-Cas9/AAV6-mediated gene editing in hematopoietic stem cells

Anastasia Conti,[1] Kety Giannetti,[1] Federico Midena,[1,2] Stefano Beretta,[1] Nicolò Gualandi,[1] Rosaria De Marco,[1,2] Edoardo Carsana,[1] Angelica Varesi,[3] Teresa Tavella,[1] Laura Alessandrini,[1,2] Parinaz Zarghamian,[4,5] Alessandra Weber,[1] Samuele Ferrari,[1] Chiara Brombin,[6] Diego Gilioli,[1,2] Lucrezia della Volpe,[1,2] Stephanie Z. Xie,[3] Ivan Merelli,[1,7] Toni Cathomen,[4,8] Luigi Naldini,[1,2] and Raffaella Di Micco[1,9,10,*]

[1]San Raffaele Telethon Institute for Gene Therapy, IRCCS San Raffaele Scientific Institute, 20132 Milan, Italy
[2]Vita-Salute San Raffaele University, 20132 Milan, Italy
[3]Princess Margaret Cancer Centre, University Health Network, Toronto, ON M5G 2J8, Canada
[4]Institute for Transfusion Medicine and Gene Therapy, Medical Center – University of Freiburg, 79106 Freiburg, Germany
[5]PhD Program, Faculty of Biology, University of Freiburg, 79104 Freiburg, Germany
[6]University Center for Statistics in the Biomedical Sciences, Vita-Salute San Raffaele University, 20132 Milan, Italy
[7]National Research Council, Institute for Biomedical Technologies, 20054 Segrate, Italy
[8]Center for Chronic Immunodeficiency (CCI), Medical Center - University of Freiburg, 79106 Freiburg, Germany
[9]University School of Advanced Studies IUSS, 27100 Pavia, Italy
[10]Lead contact
*Correspondence: dimicco.raffaella@hsr.it
https://doi.org/10.1016/j.xcrm.2025.102157

SUMMARY

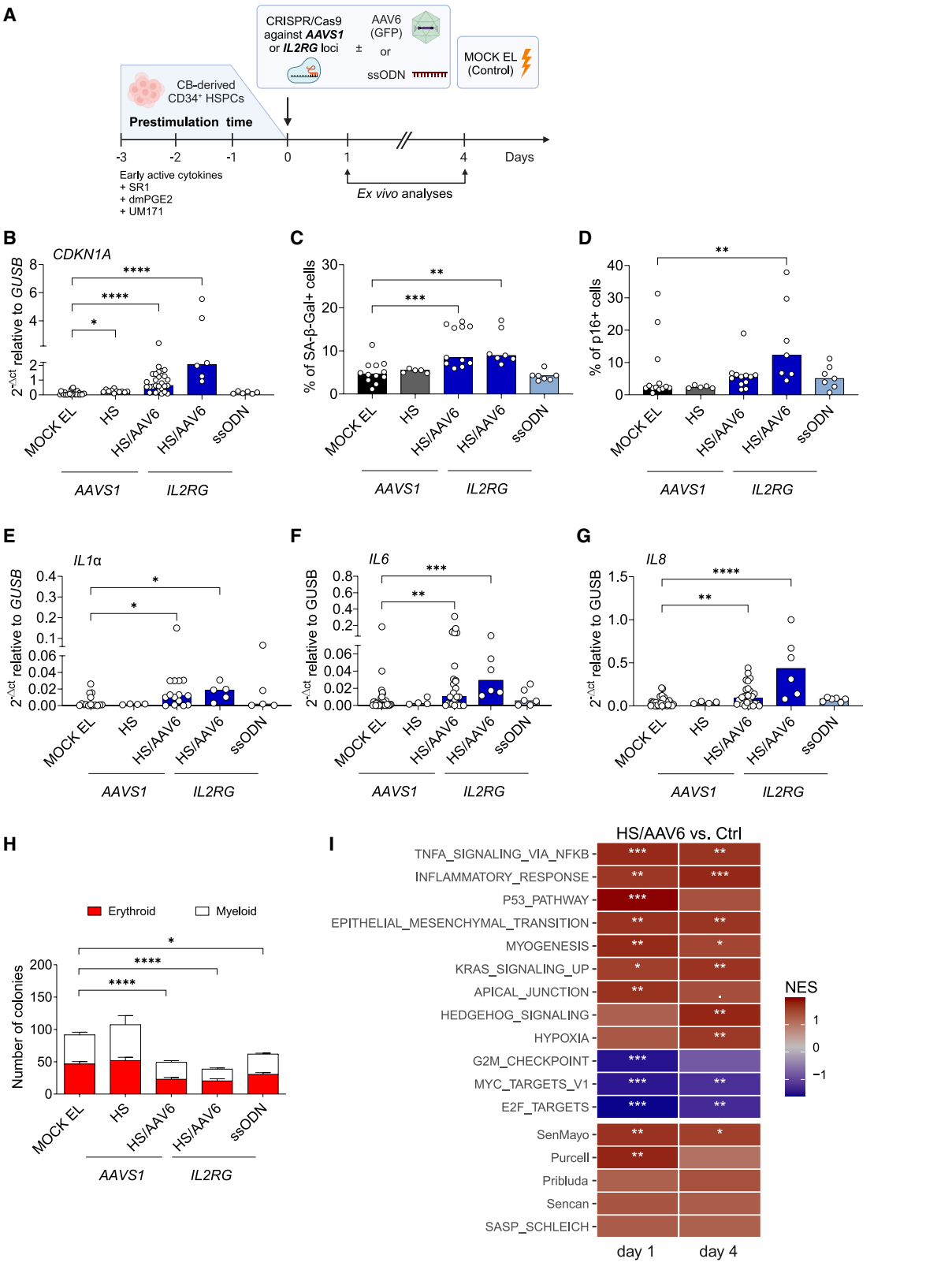
Gene editing (GE) using homology-directed repair (HDR) in hematopoietic stem and progenitor cells (HSPCs) offers promise for long-range gene correction of inherited genetic disorders. However, cellular responses induced by CRISPR-Cas9/AAV6 engineering impair the long-term repopulating potential of HDR-edited HSPCs, adversely impacting the safety and efficacy of clinical translation. Our study uncovers a durable senescence-like response in genetically engineered HSPCs triggered by p53 and interleukin (IL)-1/nuclear factor κB (NF-κB) activation, which restricts graft size and clonal diversity in long-term transplantation assays. We show that transient p53 inhibition or blocking inflammatory pathways mitigates senescence-associated responses, improving the repopulating capacity of edited HSPCs. Importantly, we identify treatment with Anakinra, an IL-1 signaling antagonist, as a promising strategy to enhance polyclonal output in HDR-edited cells while minimizing genotoxicity risks associated with the editing procedure. Overall, our findings present strategies to overcome key hurdles in HDR-based HSPC gene therapies, providing a framework for enhancing their efficacy and safety in clinical applications.

INTRODUCTION

Gene editing (GE) in hematopoietic stem and progenitor cells (HSPCs) represents a transformative gene therapy approach for immune hematological and metabolic inherited human diseases.[1–4] GE platforms, such as the CRISPR-Cas9 system, target DNA double-strand breaks (DSBs) for site-specific gene disruption or homology-mediated edits, if coupled to DNA template delivery. Corrective DNA templates can be delivered as synthetically generated non-viral single- or double-stranded oligodeoxynucleotides (ODNs),[5–7] integrase-defective lentiviral vectors (IDLVs),[8,9] or adeno-associated viral vector serotype 6 (AAV6),[10,11] with the latter being the most exploited for long-range gene correction or insertion (INS) of expression cassettes into selected genomic sites or safe harbor loci. A major constraint to efficient homology-directed repair (HDR) GE is the quiescent nature of the more primitive hematopoietic stem cells (HSCs). Optimization of *ex vivo* culture conditions,[8,12–16] promotion of cell-cycle progression to favor HDR,[14,17–20] and choice of the most appropriate delivery vehicles for DNA template[9,21–24] have only partially improved the yield of long-term repopulating HDR-edited human HSPCs. In addition, the p53-mediated DNA damage response (DDR) activated by nuclease-induced DNA DSBs acutely and adversely affects HSPC fitness,[14] and HDR-edited HSPCs show higher susceptibility to it.[15,25] AAV6 or IDLV exposure also triggers a p53 response, amplifying DSB effects and reducing clonal diversity in xenotransplants.[9,14,17,26–28] Consistent with preclinical findings, an HDR gene-editing trial using AAV6 was halted after severe hematopoietic recovery delays (https://crisprmedicinenews.com/news/graphite-bio-announces-voluntary-pause-of-phase-12-cedar-study-of-nulabeglogene-autogedtemcel-nula/).

Transient p53 inhibition during GE efficiently mitigates the detrimental effects of GE-induced DDR.[14,17] However, complete

This is an open access article under the CC BY-NC license (http://creativecommons.org/licenses/by-nc/4.0/).



(legend on next page)

p53 inactivation increased the risk of genotoxicity,[29] emphasizing the need for further safety evaluations of this approach. Although DDR-surviving HSPCs may still engraft,[17] whether they retain long-term memory of the genetic engineering procedure remains unknown. Persistent DDR signaling has been linked to cellular senescence, a condition of cell-cycle arrest in which cells undergo a profound metabolic and inflammatory rewiring.[30] Senescent cells via inflammatory molecules may contribute to myeloid skewing, chronic inflammation, and oligoclonal hematopoiesis.[31]

In this study, we uncovered that CRISPR-Cas9/AAV6-mediated long-range GE in human HSPCs induces a senescence-like phenotype and inflammatory programs that impair the functionality of HDR-edited cells. We tested strategies to prevent senescence during GE, enabling long-term polyclonal reconstitution of engineered HSPCs, and assessed their impact on genome integrity. Application of these strategies holds potential for enhancing the efficiency and safety of HDR-based clinical applications.

RESULTS

CRISPR-Cas9/AAV6-mediated GE in human HSPCs triggers cellular senescence and inflammatory programs

To study GE responses, we edited human HSPCs by electroporating Cas9 ribonucleoprotein (RNP) with a modified guide RNA (gRNA) targeting *AAVS1* or interleukin-2 receptor subunit gamma (*IL-2RG*). We delivered HDR templates via AAV6-expressing GFP or single-strand oligodeoxynucleotide (ssODN) using a 3-day prestimulation protocol.[14] Controls included only electroporated cells (MOCK ELECTRO, MOCK EL) and RNP-only conditions with a gRNA with high specificity (HS) (Figure 1A). HS/AAV6 targeting *IL2RG* achieved higher levels of GE efficiency compared to using the ssODN template and targeting the *AAVS1* locus (Figure S1A). Additionally, we found a trend of increased GFP expression in both early ($CD34^+$ CD133+) and primitive ($CD34^+$ $CD133+CD90^+$) HSPC subsets (Figure S1B). Of note, HS/AAV6-edited cells at both targeted loci displayed significantly higher expression of the DDR-related gene *CDKN1A* (*p21*) compared to MOCK EL. This upregulation was modest in HS-edited cells and in HSPCs edited using ssODN (Figure 1B). We then measured the accumulation of the senescence-associated SA-β-Galactosidase (SA-β-Gal) activity and the cell-cycle inhibitor CDKN2A (p16) (Figures S1C and S1D) and found the highest percentage of positive cells in both HS/AAV6 conditions, with no significant increase in senescence markers for ssODN and HS vs. MOCK EL, except a positive trend for p16+ in ssODN (Figures 1C and 1D). Next, we observed upregulation of senescence-associated inflammatory cytokines such as *IL-1α*, *IL-6*, *IL-8*, *CCL2*, and *CXCL10*[30–33] in both HS/AAV6 conditions compared to MOCK EL, HS, and ssODN-treated samples (Figures 1E–1G, S1E, and S1F) and increased secretion of IL-1-α, IL-1-β, growth regulated oncogene beta (GRO-β) and interferon (IFN)1-β, factors secreted when the DDR burden is heightened, as shown by treatment with a low-specificity RNP (LS)[14] (Figures S1G–S1J). Consistently, the clonogenic output of HDR-edited cells was significantly decreased, with HS/AAV6 cells more affected than ssODN (Figure 1H). Interestingly, we found a high percentage of both SA-β-Gal and p16 in the progeny of all HDR-edited cells compared to MOCK EL condition, reaching significance for both markers in the HS/AAV6 conditions and for SA-β-Gal in the ssODN experimental group (Figures S1K and S1L).

We also detected a persistent increase in cells positive for DDR foci 53BP1 and γH2AX at day 4 post-GE (Figure S1M). Transcriptional analysis and gene set enrichment analysis (GSEA) revealed significant upregulation of DDR-related genes (p53 pathway) and inflammatory response genes (tumor necrosis factor alpha [TNF-α] signaling via nuclear factor κB [NF-κB]) in HS/AAV6-edited cells, which also showed downregulation of cellular (c-MYC) and early 2 factor (E2F) targets alongside consistent upregulation of senescence-associated genes from several published gene lists[34–37] (Figure 1I).

Taken together, our analyses indicate that HDR GE, particularly with AAV6 DNA template, triggers inflammatory responses and accumulation of senescence-associated markers in human HSPCs likely downstream of an enhanced p53-mediated DDR.

HSPCs that have undergone CRISPR-Cas9/AAV6-mediated HDR display the highest accumulation of senescence markers

To test AAV6 sensing in HSPC senescence, we increased AAV6 doses (2×10^3, 1×10^4, 2×10^4 viral genome [vg]/cell) in electroporated CB HSPCs, finding that higher doses boosted HDR and reduced non-homologous end joining (NHEJ) (Figure 2A). Regardless of AAV6 dose, HS/AAV6-edited cells displayed higher accumulation of senescence markers (SA-β-Gal and p16) compared to MOCK EL, HS, and AAV6-only conditions (Figures 2B and 2C). Specifically, the highest accumulation of SA-β-Gal and p16 was observed in GFP-positive (GFP^+) cells, although a modest increase was also reported in the GFP-negative (GFP^-) cells for some conditions and senescence markers (Figures 2B and 2C). To analyze senescence and inflammatory burden across

Figure 1. CRISPR-Cas9/AAV6-mediated gene editing in human HSPCs triggers cellular senescence and inflammatory programs

(A) Experimental workflow for cord blood (CB)-derived HSPC GE.

(B) *CDKN1A* expression relative to *GUSB* housekeeping gene (n = 29, 11, 27, 6, and 6); Kruskal-Wallis test.

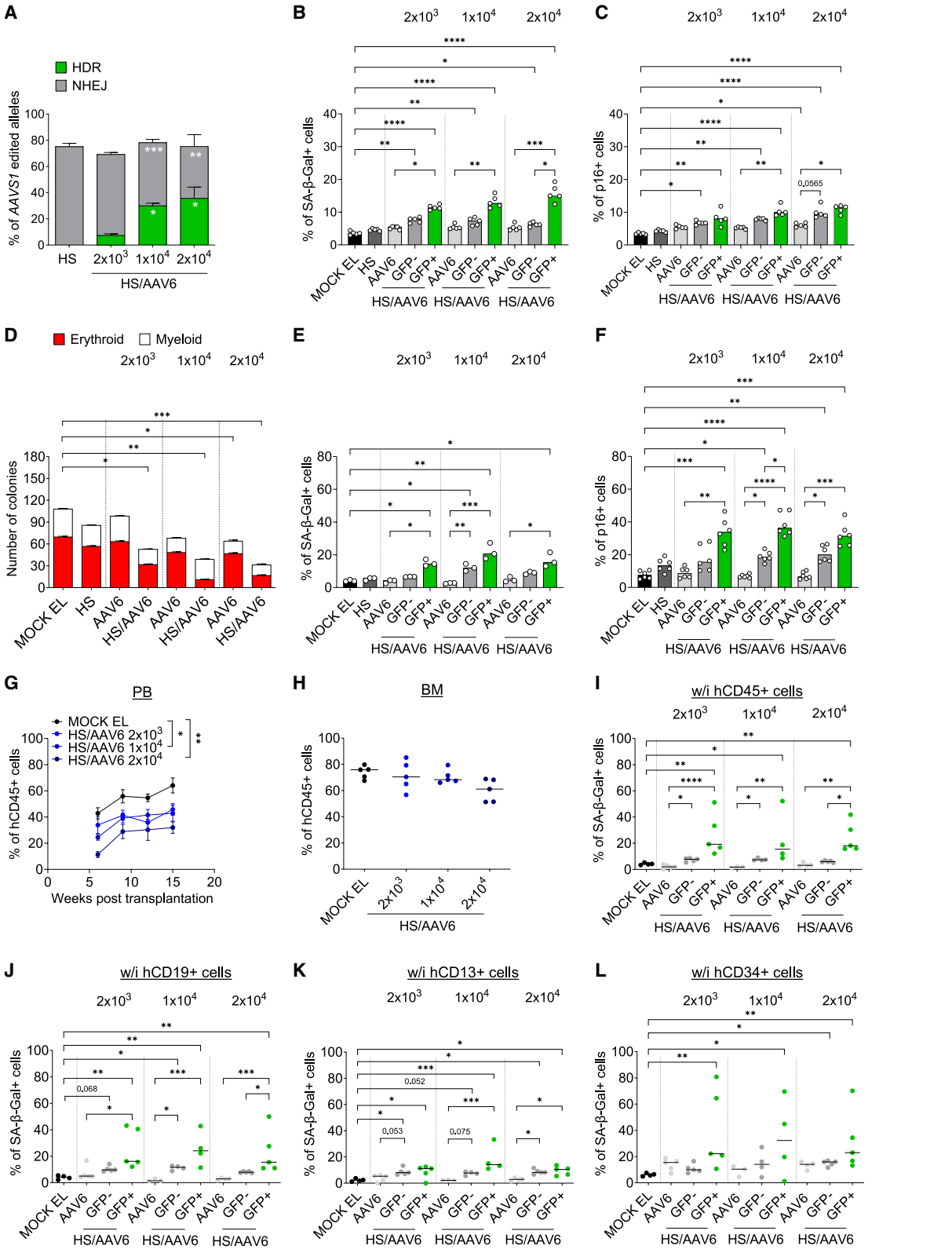
(C and D) Percentage of SA-β-Galactosidase $(SA\text{-}\beta\text{-}Gal)^+$ (C: n = 12, 5, 11, 7, and 7 for up to 8 independent donors) or $p16^+$ (D: n = 13, 5, 12, 7, and 7 for up to 9 independent donors) HSPCs; Kruskal-Wallis test.

(E–G) Inflammatory cytokine expression relative to *GUSB* housekeeping gene. (E) *IL-1α* (n = 15, 4, 15, 5, and 5); (F) *IL-6* (n = 33, 4, 27, 6, and 6); (G) *IL-8* (n = 30, 4, 27, 6, and 6); Kruskal-Wallis test.

(H) Number of colonies grown from CB-derived HSPCs treated as indicated (n = 27, 10, 18, 11, and 7); Kruskal-Wallis test; mean ± SEM.

(I) Heatmap showing normalized enrichment score (NES) from GSEA against the hallmark gene sets of the Molecular Signatures Database (MSigDB) and senescence-associated gene sets from reported literature. Terms are sorted according to NES, and adjusted p value is reported.

p values: $^*p < 0.05$; $^{**}p < 0.01$; $^{***}p < 0.001$; $^{****}p < 0.0001$. If not indicated, results are not significant (ns). Unless otherwise specified, lines indicate median values. CB HSPCs were collected at 4 days post-GE (B–H) and at 1 day and 4 days post-GE (I).



(legend on next page)

progenitor and primitive HSPC subsets, we analyzed our single-cell RNA sequencing (scRNA-seq) dataset on negative control (NEG), HS, and HS/AAV6-edited cells.[14] We found that genes from published senescence signatures[34,36,38] were enriched in GFP$^+$ cells across several cell clusters, including the more primitive HSC-enriched subsets and myeloid- and erythroid-based progenitors, with GFP$^-$ cells displaying milder but consistent increase of senescence features compared to control or HS-treated cells (Figures S2A–S2C). HS/AAV6-edited HSPCs showed reduced clonogenicity at all AAV6 doses (Figure 2D). Clonogenic output analysis revealed increased SA-β-Gal and p16 accumulation in the GFP$^+$ progeny of HS/AAV6-edited HSPCs, independently of the AAV6 dose (Figures 2E and 2F). Senescence marker accumulation also increased in the GFP$^-$ progeny of HS/AAV6-edited HSPCs, albeit to a lesser extent (Figures 2E and 2F).

Altogether, these data indicate that HDR-edited cells display the highest levels of senescence induction by cellular assays and transcriptional signatures and that senescence induction persists in the more differentiated progeny of HDR-edited HSPCs.

Senescence markers are detected *in vivo* upon transplantation of CRISPR-Cas9/AAV6-edited HSPCs

We next transplanted matching saturating number of cells exposed to increasing AAV6 doses in presence or absence of an HS RNP into immunodeficient non-obese diabetic (NOD)-severe combined immunodeficiency (SCID)-IL2Rg$^{-/-}$ (NSG) mice. We found that, only when higher doses of AAV6 were employed (Figures 2G and S2D), the levels of engraftment in the peripheral blood (PB) were significantly reduced over time. At 15 weeks endpoint, we found only a trend toward lower engraftment for high-dose HS/AAV6 condition with respect to the MOCK EL group in the bone marrow (BM) and spleen (SP), with almost comparable lineage output across all conditions (Figures 2H and S2E–S2H). When analyzing SA-β-Gal level (Figures S2I), we noted the highest accumulation in GFP$^+$ cells over MOCK EL or AAV6-only conditions across all hematopoietic subpopulations and within the HSPC compartment (CD34$^+$ cells) (Figures 2I–2L). Notably, in GFP$^-$ cells, we found a modest yet consistent increase in SA-β-Gal$^+$ cells in the human graft (hCD45$^+$ cells) and in differentiated B cell (hCD19$^+$ cells) and myeloid (hCD13$^+$ cells) progeny (Figures 2I–2K). To quantify the senescence burden *in vivo* in the early and late phases of hematopoietic reconstitution, we analyzed mice transplanted with HS or HS/AAV6 HSPCs at 6 and 15 weeks post-transplantation. We found significantly lower levels of engraftment in BM and SP at 6 weeks post-transplantation for HS/AAV6 vs. HS conditions (Figures 3A and S3A), with no significant differences in the lineage output in the BM and increased myeloid output at the expense of B and T cells in the SP (Figures S3B and S3C). Moreover, we observed a marked accumulation of SA-β-Gal specifically in the GFP$^+$ BM-derived HSPCs from the HS/AAV6 group at both early and later time points post-transplantation (Figure 3B), which negatively correlated with the percentage of their engraftment (Figures 3C and 3D). To rule out the possibility that the observed senescence induction was exacerbated by the expression of an exogenous GFP, we tested an AAV6 bearing an alternative reporter cassette expressing the clinically compatible truncated form of the low-affinity nerve growth factor receptor (ΔLNGFR) reporter,[39] yielding comparable GE efficiencies across HSPC subsets (Figures S3D and S3E). We found similarly low clonogenic potential and accumulation of senescence markers in the progeny of HS/AAV6 HSPCs, independently from the reporter cassette employed (Figures S3F–S3H). *In vivo*, cells edited with either template did not show significant differences in engraftment in PB, BM, and SP of transplanted mice (Figures 3E, 3F, and S3I). However, in the BM, ΔLNGFR-edited HSPCs exhibited increased B cell output at the expense of myeloid lineage compared to the GFP-edited HSPCs, with similar graft composition observed in the SP (Figures S3J and S3K). Additionally, there was similar accumulation of SA-β-Gal$^+$ cells in PB over time and in HDR-edited BM-derived HSPCs at the endpoint (Figures 3G and 3H).

We next evaluated senescence induction in mobilized peripheral blood (mPB)-derived adult HSPCs post-GE by targeting both *AAVS1* and *IL2RG* genomic loci and found HDR GE efficiencies up to 20% and concomitant reduction in NHEJ for both targeted loci (Figure S4A). We confirmed the higher induction of *p21* (Figure S4B) and the accumulation of DDR foci (Figure S4C) in mPB HS/AAV6-edited cells with respect to MOCK EL, HS, and AAV6-only conditions. Moreover, we observed a preferential accumulation of SA-β-Gal and p16 in HS/AAV6 GFP$^+$ cells (Figures 4A and 4B) and of SA-β-Gal in HS/AAV6 GFP$^-$ cells 4 days post-GE compared to MOCK EL, HS, and AAV6-only conditions. Although no significant changes in cell composition were observed across conditions, differences were noted between the different donors edited for the two loci (Figure S4D). Senescence induction was associated with a reduction in clonogenic potential of HS/AAV6 cells

Figure 2. HSPCs that have undergone CRISPR-Cas9/AAV6-mediated HDR display the highest accumulation of senescence markers

(A) Percentage of HDR- and NHEJ-edited alleles in CB-derived HSPCs with increasing doses of AAV6 vector or HS RNP. HDR: 2×10^3: $n = 2$, 1×10^4: $n = 27$, 2×10^4: $n = 4$. NHEJ: HS: $n = 7$, 2×10^3: $n = 2$, 1×10^4: $n = 11$, 2×10^4: $n = 4$; Kruskal-Wallis test; mean ± SEM.

(B and C) Percentage of SA-β-Gal$^+$ (B) or p16$^+$ (C) CB-derived HSPCs ($n = 5$ technical replicates); Friedman test.

(D) Number of colonies grown from CB-derived HSPCs treated as indicated ($n = 3$ independent CFU replicates); Friedman test; mean ± SEM.

(E and F) Percentage of SA-β-Gal$^+$ (E, $n = 3$ independent CFU replicates) or p16$^+$ (F, $n = 6$ independent CFU replicates) cells in the progeny of edited CB-derived HSPCs at indicated conditions; Friedman test.

(G) Percentage of hCD45$^+$cells in PB of mice transplanted with CB-derived HSPCs edited with increasing AAV6 doses ($n = 5$). Linear mixed effects models (LME) followed by *post hoc* analysis; results are shown for the last time point; mean ± SEM.

(H) Percentage of BM-derived hCD45$^+$ cells in mice in (G) ($n = 5$); Kruskal-Wallis test.

(I–L) Percentage of SA-β-Gal$^+$ cells in BM-derived human CD45$^+$ (I), CD19$^+$ (J), CD13$^+$ (K), and CD34$^+$ (L) ($n = 4, 5, 5, 5, 3, 4, 4, 4, 5$, and 5 of mice in H and Figure S2E); Kruskal-Wallis test.

p values: *$p < 0.05$; **$p < 0.01$; ***$p < 0.001$; ****$p < 0.0001$. If not indicated, results are not significant (ns). Unless otherwise specified, lines indicate median values. Samples were collected at 4 days post-GE (A–F) and at 15 weeks post-transplantation (H–L).

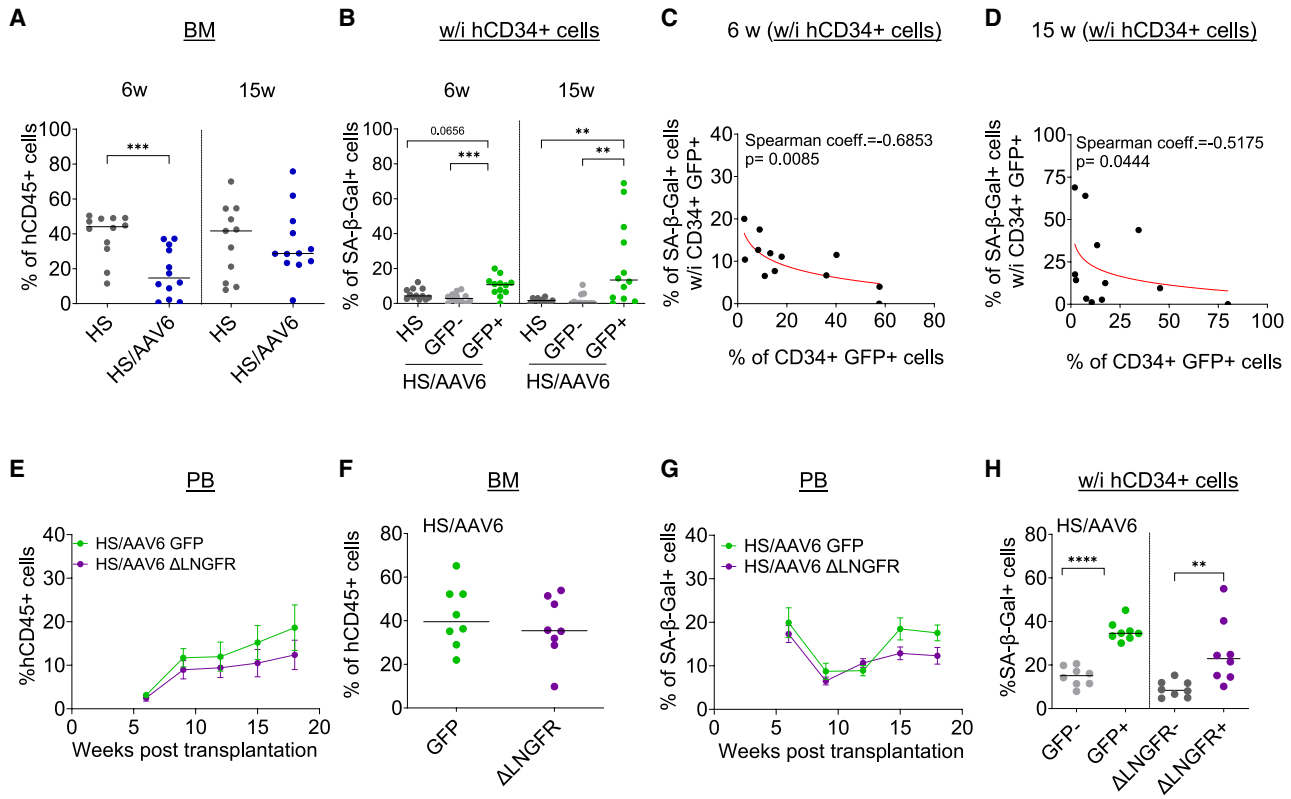


Figure 3. Senescence markers are detected *in vivo* upon transplantation of CRISPR-Cas9/AAV6-edited HSPCs

(A) Percentage of hCD45$^+$ cells in BM early (6 weeks, 6w) and late (15 weeks, 15w) post-transplantation of mice transplanted at day 1 post-GE with CB-derived HSPCs. (6 weeks: n = 12 and 12; 15 weeks: n = 11 and 12); Mann-Whitney test.

(B) Percentage of SA-β-Gal$^+$ cells in BM-derived CD34$^+$ HSPCs retrieved from mice in (A) (n = 12, 12, 12, 12, 12, and 11); Kruskal-Wallis test.

(C and D) Spearman correlation between the percentage of SA-β-Gal$^+$ cells within CD34$^+$ GFP$^+$ cells (y axis) and CD34$^+$ GFP$^+$ (x axis) at 6 weeks (C) or 15 weeks (D) post-transplantation (n = 12). Each dot represents an individual mouse from (B).

(E) Percentage of hCD45$^+$ cells in PB over time of mice transplanted at day 1 post-GE with CB-derived HSPCs treated as indicated (n = 8). LME followed by *post hoc* analysis; results are shown for the last time point; mean ± SEM.

(F) Percentage of BM-derived hCD45$^+$ cells of mice from (E) (n = 8); Mann-Whitney test.

(G) Percentage of hCD45$^+$SA-β-Gal$^+$ cells in PB of mice from (E) (n = 8); LME followed by *post hoc* analysis; mean ± SEM.

(H) Percentage of SA-β-Gal$^+$ cells in BM-derived hCD34+ of mice from (F) (n = 8); Mann-Whitney test.

p values: **p < 0.01; ***p < 0.001; ****p < 0.0001. If not indicated, results are not significant (ns). Unless otherwise specified, lines indicate median values, and samples were collected at 18 weeks post-transplantation (F and H).

(Figures 4C and S4E), while p16 levels also increased in the progeny of HS/AAV6 GFP$^+$ HSPCs edited at the two loci (Figure S4F). Finally, we transplanted GE mPB HSPCs into NSG mice. Although the kinetics of PB reconstitution significantly differed from those observed with CB-derived HSPCs, we observed a significantly reduced engraftment for the HS/AAV6 condition compared to other groups early post-transplant (6 weeks) and increase in the HS over MOCK EL conditions (Figure 4D), without detectable difference in the engraftment in BM and SP at the endpoint (15 weeks) likely due to high engraftment variability among mice (Figures 4D, 4E, and S4G). Despite no significant differences in the lineage output in BM (Figure S4H), we reported a significant increase in B cells at the expense of T cells in the SP at the endpoint in HS/AAV6 compared to MOCK EL conditions (Figure S4I). Notably, GFP$^+$ cells showed substantially higher accumulation of SA-β-Gal across hematopoietic subpopulations (Figures 4F–4H). Similarly, GFP$^+$ BM-derived HSPCs at the endpoint displayed higher accumulation of SA-β-Gal and p16, reaching up to 60% in some samples (Figures 4I and 4J).

Overall, these data highlight that the senescence-like phenotype in HS/AAV6-edited cells persists after transplantation, at both early and late stages of hematopoietic reconstitution. This persistence was most pronounced in HDR-edited cells and their progeny, regardless of the reporter cassette for HDR or the HSPC source.

p53 inhibition or anti-inflammatory treatments at the time of GE mitigate senescence response and improve HSPC fitness

We tested whether transient modulation of DDR and inflammatory-related transcriptional signatures identified in HDR-edited cells could alleviate the long-lasting senescence burden in HS/AAV6-edited HSPCs and their progeny (Figure 5A). We first administered at the time of GE Anakinra (ANAK), a clinically approved recombinant receptor antagonist of IL-1,[40] a cytokine involved in HSC

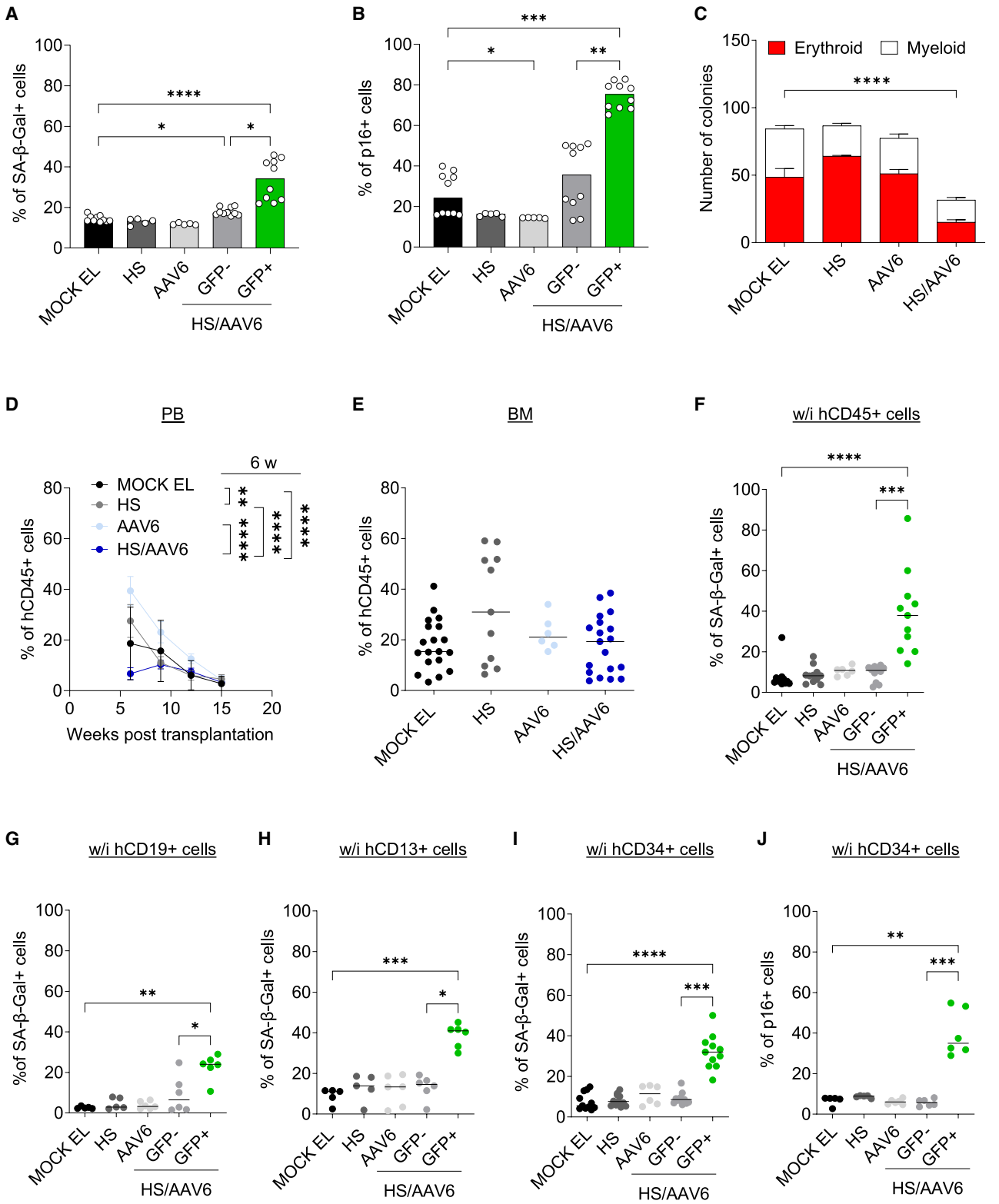


Figure 4. Senescence markers are detected *in vivo* upon transplantation of CRISPR-Cas9/AAV6-edited HSPCs

(A and B) Percentage of SA-β-Gal$^+$ (A) or p16$^+$ (B) mPB HSPCs (n = 10, 5, 5, 10, and 10 for up to 3 independent donors); Kruskal-Wallis test.

(C) Number of colonies grown from mPB HSPCs treated as indicated (n = 9, 3, 3, and 9 for up to 3 independent donors); Kruskal-Wallis test; mean ± SEM.

(legend continued on next page)

exhaustion and DDR-dependent inflammation and a key component of the senescence-associated inflammatory programs.[41,42] Transcriptional analysis of ANAK-treated GE HSPCs displayed a downregulation of genes associated with IFN responses (IFN-alpha response and IFN-gamma response) and NF-κB-related inflammatory pathways (e.g., IL-2_STAT5 signaling, IL-6_JAK_STAT3 signaling, and TNF-α signaling via NF-κB) at early and late time points post-GE (Figure 5B). Consistently, we reported downregulation of the senescence-associated pro-inflammatory cytokines *IL-1A*, *IL-8*, and *IL-6* in ANAK-treated HS/AAV6-edited cells compared to the HS/AAV6 condition (Figures S5A–S5C). Furthermore, we reported increased nuclear localization of NF-κB specifically in HS/AAV6-edited HSPCs, which was mitigated by ANAK treatment (Figures S5D and S5E). Therefore, we reasoned to target NF-κB signaling by employing the inhibitor of nuclear factor-κB kinase (IKK)-2 Inhibitor (SC514) at the time of GE[43] and found that its administration reduced pro-inflammatory gene expression in edited HSPCs (Figure S5F), thus partly mimicking the effects of ANAK.

We next administered together with HS/AAV6 an mRNA encoding for a p53-dominant negative form (GSE56)[14,44] alone or in combination with anti-inflammatory treatments. Treatments with GSE56, ANAK, or SC514 alone or combination of ANAK or SC514 with GSE56 at the time of GE did not affect the GE efficiency on CB-derived HSPC subsets across multiple experiments, nor the extent of HDR (Figures S5G and S5H). Notably, all treatments decreased the accumulation of the senescence markers SA-β-Gal and p16, particularly in HDR-edited (GFP^+) cells, reaching statistical significance for ANAK and SC514 treatments and the highest *p* value when the latter was combined with GSE56 (Figures 5C and 5D). We also observed increased clonogenic potential associated with a reduced senescence burden in the progeny of GE HSPCs, more pronounced in the GFP^+ cells of the ANAK and SC514+GSE56 conditions (Figures 5E–5G). Most findings were recapitulated in GE mPB-derived HSPCs, where we observed increased nuclear localization of NF-κB in the AAV6-only condition respect to MOCK EL, reaching higher levels in the HS/AAV6 condition (Figure S5I). All mitigating treatments significantly reduced NF-κB levels in HS/AAV6 cells without major changes in HDR efficiency in bulk HSPCs and across subsets (Figures S5J and S5K), reduced SA-β-Gal levels in GFP^+ cells in liquid culture (Figure 5H), ameliorated the clonogenic potential of HS/AAV6 cells (Figure 5I), and reduced SA-β-Gal accumulation in their clonogenic output to similar extents, reaching or just approaching statistical significance (Figure 5J).

Taken together, these findings reveal that GSE56, ANAK, or SC514, alone or in combination at the time of GE, rescue HSPC clonogenic potential *ex vivo*, with concomitant mitigation of senescence responses mainly in HDR-edited cells regardless of the HSPC source.

Mitigation of senescence enhances *in vivo* polyclonal hematopoietic reconstitution by HDR-edited HSPCs

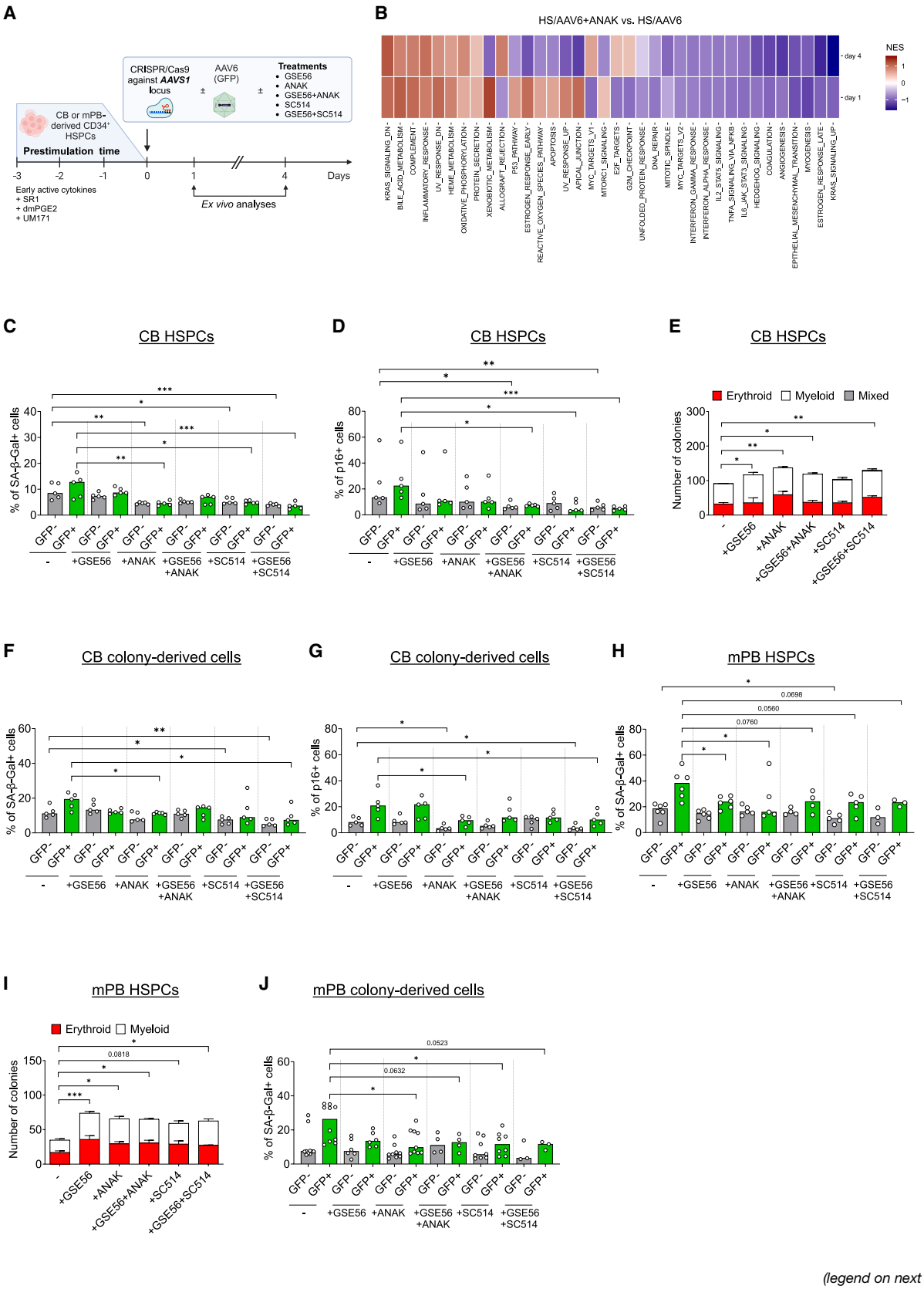
To investigate the benefit of inhibiting GE-induced p53 and IL-1 signaling pathways on the repopulating potential of HSPCs, we transplanted matched saturating cell doses of CB-derived HSPCs edited for HDR with or without ANAK, GSE56, or the combination of the two. Human engraftment was high in all samples from PB, BM, and SP (Figures 6A, 6C, and S6A), with a trend toward increased engraftment in PB observed with GSE56. HDR-edited human cells (hCD45+ GFP^+) were significantly more in PB when HSPCs were edited in the presence of GSE56 or GSE56 co-administered with ANAK, with a trend for increase also when ANAK was administered alone (Figure 6B). We also found increased HDR-edited cells in BM across all treatments, which reached significance for ANAK alone or in combination with GSE56 (Figure 6D), in line with higher levels of GFP^+ cells found within the different hematopoietic lineages in BM (Figure 6E). In the SP, all mitigating treatments increased the fraction of GFP^+ cells, especially in the B and myeloid compartments (Figure S6B). Intriguingly, we observed a trend for decreased SA-β-Gal levels in BM HDR-edited HSPCs, which reached significance with the combination of ANAK and GSE56 (Figure 6F). When plated in colony-forming units (CFUs), cells from the BM of mice transplanted with HSPC GE with mitigating treatments formed significantly more colonies compared to those with no treatment (Figure 6G). Interestingly, secondary transplantation showed serial engraftment of HDR-edited cells across all conditions up to 13 weeks (Figures S6C–S6F), and we reported a significant reduction of senescence markers in the HDR-edited fraction in mice receiving cells edited in the presence of GSE56, ANAK, or the combination of the two (Figure S6G).

We next assessed whether ANAK, GSE56, or NF-κB inhibitor (SC514) treatments could improve hematopoietic repopulation and mitigate senescence responses even when transplanting matched lower cell doses of edited cells. While only GSE56 treatment improved the total engraftment of human HSPCs in PB and BM (Figures S6H and S6I), with a trend for increased percentage of HDR-edited cells across lineages (Figures S6J and S6K), all treatments showed significant reduction of senescence markers in HDR-edited HSPCs retrieved from transplanted animals (Figures S6L and S6M).

We evaluated the impact of mitigating treatments on the repopulating potential of mPB-derived GE HSPCs and found that GSE56 treatment significantly improved their engraftment in PB, with a trend of increase in the BM (Figures 6H and 6I). Additionally, GSE56 treatment, either alone or in combination with ANAK, increased the fraction of HDR-edited cells in the PB early post-transplant, whereas SC514 reduced this fraction (Figure 6J). Despite lower human engraftment at the endpoint

(D) Percentage of $hCD45^+$ cells in PB of mice transplanted with mPB HSPCs at day 1 post-GE at the indicated conditions (n = 19, 11, 6, and 19). LME followed by *post hoc* analysis; results are shown for the 6 weeks post-transplantation time point; mean ± SEM.
(E) Percentage of BM-derived $hCD45^+$ cells in mice from (D) (n = 19, 11, 6, and 19); Kruskal-Wallis test.
(F–J) Percentage of SA-β-Gal^+ (F–I) or $p16^+$ (J) cells within human $CD45^+$ (F: n = 11, 11, 6, 11, and 11), $CD19^+$ (B cells, G: n = 5, 5, 6, 6, and 6), $CD13^+$ (myeloid cells, H: n = 5, 5, 6, 6, and 6), and $CD34^+$ (HSPCs, I: n = 11, 11, 6, 11, and 11 and J: 5, 5, 6, 6, and 6) retrieved from the BM of mice from either one or two independent experiments from (E) 15 weeks post-transplantation; Kruskal-Wallis test; median.
p values: $^*p < 0.05$; $^{**}p < 0.01$; $^{***}p < 0.001$; $^{****}p < 0.0001$. If not indicated, results are not significant (ns). Unless otherwise specified, lines indicate median values, and mPB HSPCs were collected at 4 days post-GE (A–C) and 18 weeks post-transplantation (D–J).

CellPress
OPEN ACCESS



(legend on next page)

(15 weeks) across all conditions, only ANAK treatment increased the fraction of edited cells in the PB at this time point (Figure 6J). At the endpoint in the BM, however, all mitigating treatments showed a trend toward higher levels of engrafted GFP$^+$ cells (Figure 6K) and led to a significantly lower percentage of senescent cells within the human graft either in PB over time or in BM-derived HSPCs at the endpoint (Figures 6L and 6M) and a consistent trend for higher clonogenic potential upon rechallenging into semisolid medium (Figure 6N).

We next evaluated the clonality of edited graft. By deep sequencing the *AAVS1* locus and measuring insertion or deletion (indel) diversity as a surrogate readout of *in vivo* clonality of cells that underwent NHEJ-mediated repair of the edit, we found a comparable number of unique indels across conditions (Figure 6O). To assess the clonal composition of HDR-edited HSPCs, we performed clonal tracking by using an AAV6 repair template pool with a heritable "barcode" sequence (BAR) downstream of the GFP reporter cassette.[17] Significantly enhanced long-term polyclonal reconstitution of HDR-edited cells in the BM was observed for GSE56 and ANAK treatments (Figure 6P).

Collectively, our data imply that p53 inhibition or IL-1-mediated anti-inflammatory treatments during GE of CB and mPB-derived HSPCs substantially reduce the fraction of cells acquiring a lasting senescence-like phenotype and rescue a polyclonal contribution of HDR-edited HSPCs to both early and long-term graft.

ANAK treatment reduces the genotoxicity risk associated with the GE procedure

We finally asked whether p53 inhibition or anti-inflammatory treatments affect the genotoxicity risk of GE. Using a dual-targeting RNP that cleaves both the intended *IL2RG* locus (on chromosome X) and also a second genomic off-target site with moderate cleavage activity (on chromosome 14),[14] we quantified translocation events between these 2 target sites in the clonogenic output of HS/AAV6-edited cells. We found a negligible fraction of colonies bearing a translocation event, without detectable difference when using GSE56, ANAK, or SC514 regardless of the HSPC source (Figure S7A). CAST-Seq analysis on mPB-derived HSPCs[45] confirmed no increase in translocation events or on-target aberrations with CRISPR-Cas9 GE (HS) in the presence of GSE56 or anti-inflammatory compounds (Figures 7A and S7B; Table S2). Micronuclei formation[46] significantly increased in the HS/AAV6 conditions (Figures S7C and S7D), and there was no significant difference in micronuclei-bearing cells with GSE56, but a consistent reduction was observed with ANAK or SC514 in both HSPC cell sources (Figures S7C and S7D).

To evaluate large deletions (DELs) downstream the target site, we screened around 500 randomly picked colonies from the outgrowth of HS/AAV6 *AAVS1*-edited cells[9] with or without GSE56, ANAK, and SC514 in CB and mPB HSPCs. In mPB HSPCs, DELs increased downstream of the *AAVS1* cut site in the HS/AAV6 condition, compared to unedited cells, and were further increased with GSE56, while ANAK and SC514 significantly reduced them (Figure 7B). A similar trend across treatments was observed in GE CB HSPCs (Figure 7C).

Recent studies investigated the possibility of selecting harmful and potentially oncogenic mutations during CRISPR-Cas9 GE across cell types.[47,48] Thus, we assessed the mutational rates in the human graft by performing ultra-high coverage (500X) whole-exome sequencing (WES). p53 inhibition or SC514 treatement increased the mutational rate, while ANAK treatment resulted in a lower rate (Figure 7D). We found overall similar patterns of variant types such as single-nucleotide variants (SNVs), DELs, and INSs across all experimental groups (Figure 7E) with comparable frequencies of different SNV types across treatments (Figure 7F). When analyzing the functional impact of the reported mutations,[49] we observed a similar percentage of high-, medium-, and low-impact mutations across all conditions (Figure 7G). As progressively exhausting genetically engineered HPSCs may eventually accumulate mutations associated with clonal hematopoiesis (CH),[50] we also analyzed the impact of GE on genes involved in CH (Table S3) and found comparable number of CH mutations across treatments compared to untreated HS/AAV6 HSPCs (Figures 7H and S7E). Instead, when we assessed the mutational burden on a panel of 182 cancer-associated genes (Table S4), we reported a significantly lower mutational rate specifically upon performing GE in the presence of ANAK (Figures 7I and S7F).

In conclusion, our findings show that GSE56 treatment might increase the occurrence of potential genotoxic events following GE. Conversely, ANAK treatment effectively reduced large DELs, micronuclei, and the overall mutational burden in transplanted GE HSPCs.

DISCUSSION

By integrating cellular-based and molecular assays, we identified the activation of a senescence-like program in human CRISPR-Cas9/AAV6 gene-edited HSPCs. We propose that the

Figure 5. p53 inhibition or anti-inflammatory treatments at the time of gene editing mitigate senescence response and improve HSPC fitness

(A) Experimental workflow.

(B) Heatmap showing NES from GSEA against the hallmark gene sets of the Molecular Signatures Database (MSigDB). Terms are sorted according to NES.

(C and D) Percentage of SA-β-Gal$^+$ (C) or p16$^+$ (D) CB HSPCs treated as indicated at day 4 post-GE (n = 5 technical replicates); Friedman test.

(E) Number of colonies grown from CB HSPC gene edited and treated as indicated at day 4 post-GE (n = 5 independent CFU replicates); Friedman test; mean ± SEM.

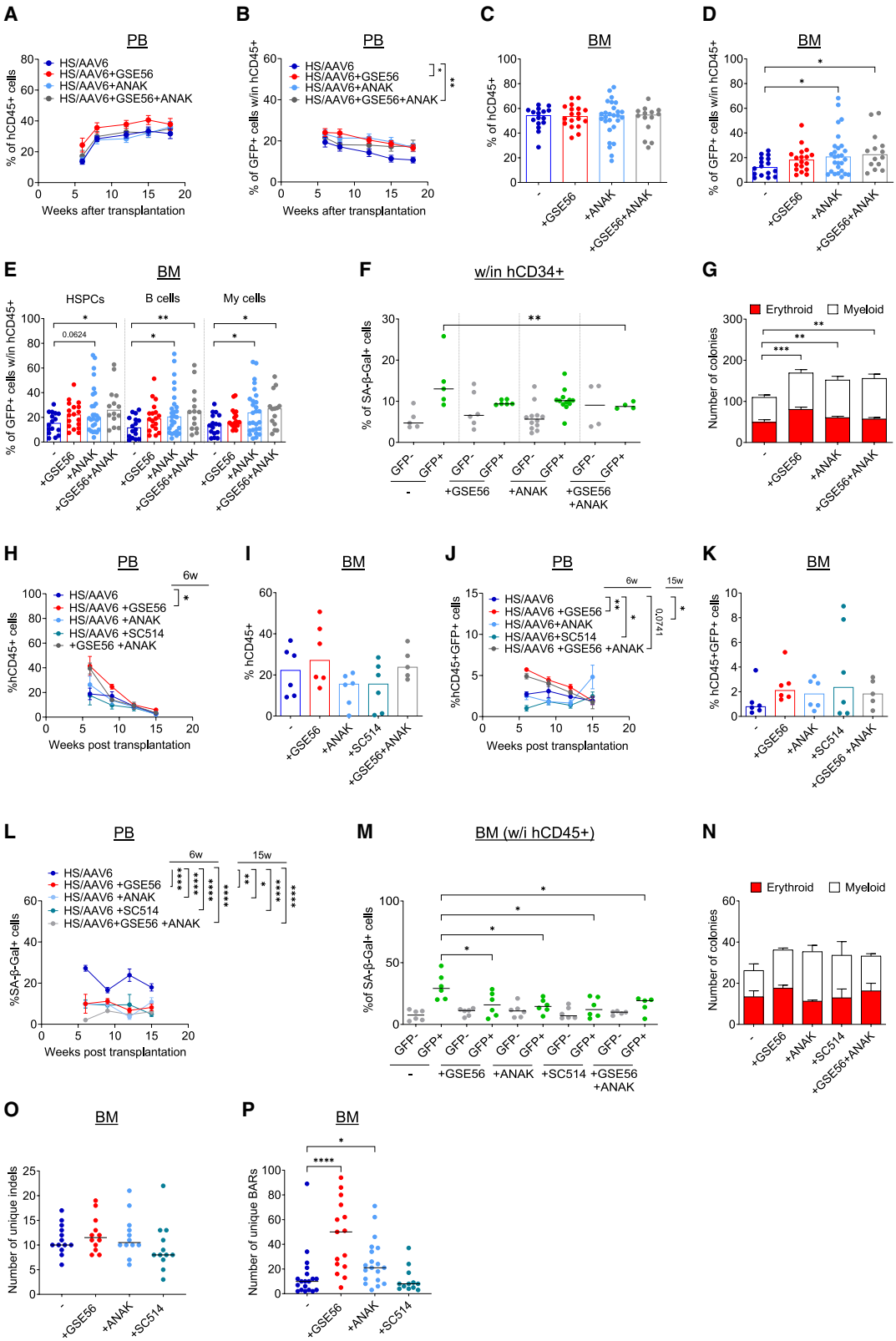
(F and G) Percentage of SA-β-Gal$^+$ (F) or p16$^+$ (G) cells in the progeny of edited CB HSPCs at indicated conditions from (E) (n = 5 independent CFU replicates); Friedman test.

(H) Percentage of SA-β-Gal$^+$ mPB HSPCs treated as indicated (n = 6, 6, 6, 6, 5, 5, 4, 4, 5, 5, 3, and 3); Kruskal-Wallis test.

(I) Number of colonies grown from mPB HSPCs treated as indicated (n = 5, 6, 4, 4, 4, and 3); Kruskal-Wallis test; mean ± SEM.

(J) Percentage of SA-β-Gal$^+$ cells in the progeny of edited mPB HSPCs at indicated conditions (n = 10, 10, 6, 6, 9, 9, 4, 4, 8, 8, 3, and 3); Kruskal-Wallis test.

p values: *$p < 0.05$; **$p < 0.01$; ***$p < 0.001$. If not indicated, results are not significant (ns). Unless otherwise specified, lines indicate median values, and HSPCs were collected at 4 days post-GE (C–J) and at day 1 and 4 post-GE (B). (−): HS/AAV6 condition.



(legend on next page)

pronounced induction of this program in HDR cells (evidenced by GFP+ or ΔLNGFR+ subsets) likely reflects the susceptibility of HDR-permissive cells in the S-phase to the combined stress of nuclease-induced DSBs and AAV6 sensing. This aligns with previous studies in murine and human HSPCs, which highlight that (1) the transition from quiescence to cell-cycle entry can lead to DNA damage *per se*,[51] (2) HSCs in S-phase may encounter increased DNA replication fork stalling and consequent dysfunction,[52] and (3) DSB induction has a stronger impact on the transcriptional landscape of HSPCs in S/G2 cycle phases.[14,15,53]

Since a single genetically modified HSPC can repopulate a mouse, the impact of senescence on hematopoietic reconstitution has been overlooked. We show that senescence-related programs initiated *ex vivo* persist even after secondary transplantation. Notably, senescence features appear to be transmitted from progenitors to their differentiated progeny, either through direct engraftment of senescent cells[54] or by altering the niche environment via inflammatory signaling, inducing senescence-like traits in neighboring cells.[31] We report that targeting the IL-1/NF-κB signaling pathway improves the functional properties and clonal output of long-term repopulating GE HSPCs, consistent with previous studies showing that IL-1 regulates senescence-associated inflammatory program[55] and negatively impacts HSPC clonogenic and repopulating potential.[31,56] Notably, blocking IL-1 signaling in old mice restores a balanced hematopoietic reconstitution by HSCs reducing their inflammatory phenotype.[57] The finding that ANAK recovers the overall hematopoietic output of HDR-edited HSPCs might be explained by the preservation of functional long-term repopulation-competent HSCs in response to GE-induced DDR, consistent with reports highlighting that ANAK protects hematopoietic cells from DNA damage.[58,59] However, we cannot exclude that the apparent rescue of a greater number of normally functioning stem cells following anti-inflammatory treatments is due to better preservation of more committed progenitors, whose improved function indirectly supports more primitive stem cell population recovery.

GE procedure carries intrinsic genotoxicity risks associated with human diseases and cancer.[46,60] Since senescence acts as tumor suppressor mechanism, its modulation by p53 or inflammatory pathways inhibition could impose a potential additional genotoxicity risk in GE cells. Consistent with the recently reported increase in genomic aberrations in p53 knockout cells treated for CRISPR-Cas9 GE,[29] we observed an increase in large DELs and mutational burden upon transient p53 inhibition. This highlights the need for further investigations of the effects of transient p53 inhibition when moving toward clinical applications. Notably, the increased variants retrieved for engrafting HSPCs edited with p53 inhibitor likely reflect higher engraftment for this condition, where accumulation of spontaneous variants may provide a surrogate readout of clonality. Strikingly, ANAK treatment significantly reduced all measured genotoxicity readouts, suggesting a protective effect that may mitigate DNA damage or promote more precise DNA repair. Importantly, ANAK's beneficial effects on HSPC genome integrity align with studies showing that inflammatory stimuli promote leukemogenesis through deamination via increased activity of APOBEC3C and ADAR1[61,62] and that IL-1 is a DNA damage stressor linked to genotoxic stress and inflammation.[63] Although further investigations are needed before its clinical translation in disease settings, ANAK's clinical approval and tolerability for inflammatory disorders[40] may accelerate its use in GE to enhance stable engraftment of long-term HDR-corrected cells.

In conclusion, our findings uncover senescence and inflammatory programs as adverse long-term consequences of HDR-mediated GE in human HSPCs with fundamental implications for developing safer and more efficient HSPC-based clinical application.

Figure 6. Mitigation of senescence enhances *in vivo* polyclonal hematopoietic reconstitution by HDR-edited HSPCs

(A and B) Percentage of hCD45$^+$ (A) or GFP$^+$ hCD45$^+$ (B) cells in PB of high-cell-dose transplanted mice at day 1 post-GE with CB-derived HSPCs treated as indicated (n = 17, 18, 27, and 14). LME followed by *post hoc* analysis; results are shown for the 18 weeks post-engraftment time point; mean ± SEM.

(C–E) Percentage of hCD45$^+$ (C); GFP$^+$ hCD45$^+$ (D); or GFP$^+$ HSPCs (CD34$^+$), B cell (CD19$^+$), and myeloid cells (CD13$^+$) (E) in BM of transplanted mice from (A) (n = 16, 18, 27, and 14); Kruskall-Wallis test.

(F) Percentage of SA-β-Gal$^+$ cells in BM-derived CD34$^+$ retrieved from mice transplanted with high cell doses (n = 5, 5, 6, 6, 12, 12, 4, and 4 from one independent experiment from C); Kruskal-Wallis test.

(G) Number of colonies grown from BM-derived CD34$^+$ HSPCs from (C) of mice treated as indicated 18 weeks post-transplantation (n = 13, 14, 20, and 14); Kruskal Wallis test; mean ± SEM.

(H) Percentage of hCD45$^+$ cells in PB of mice transplanted at day 1 post-GE with mPB HSPCs treated as indicated (n = 6, 6, 6, 6, and 5). LME followed by *post hoc* analysis; results are shown for the 6 weeks post-engraftment time point; mean ± SEM.

(I) Percentage of BM-derived hCD45$^+$ cells in mice shown in (H) at 15 weeks post-transplantation. (n = 6, 6, 6, 6, and 5); Kruskal-Wallis test.

(J) Percentage of hCD45$^+$ GFP$^+$ cells in PB of mice from (H). LME followed by *post hoc* analysis; results are shown for the 6- and 15-week post-transplantation time points; mean ± SEM.

(K) Percentage of hCD45$^+$GFP$^+$ cells in BM of mice shown in (I) at 15 weeks post-transplantation; Kruskal-Wallis test.

(L) Percentage of SA-β-Gal$^+$ cells in PB of mice shown in (H). LME followed by *post hoc* analysis; results are shown for the 6 and 15 weeks post-transplantation time points; mean ± SEM.

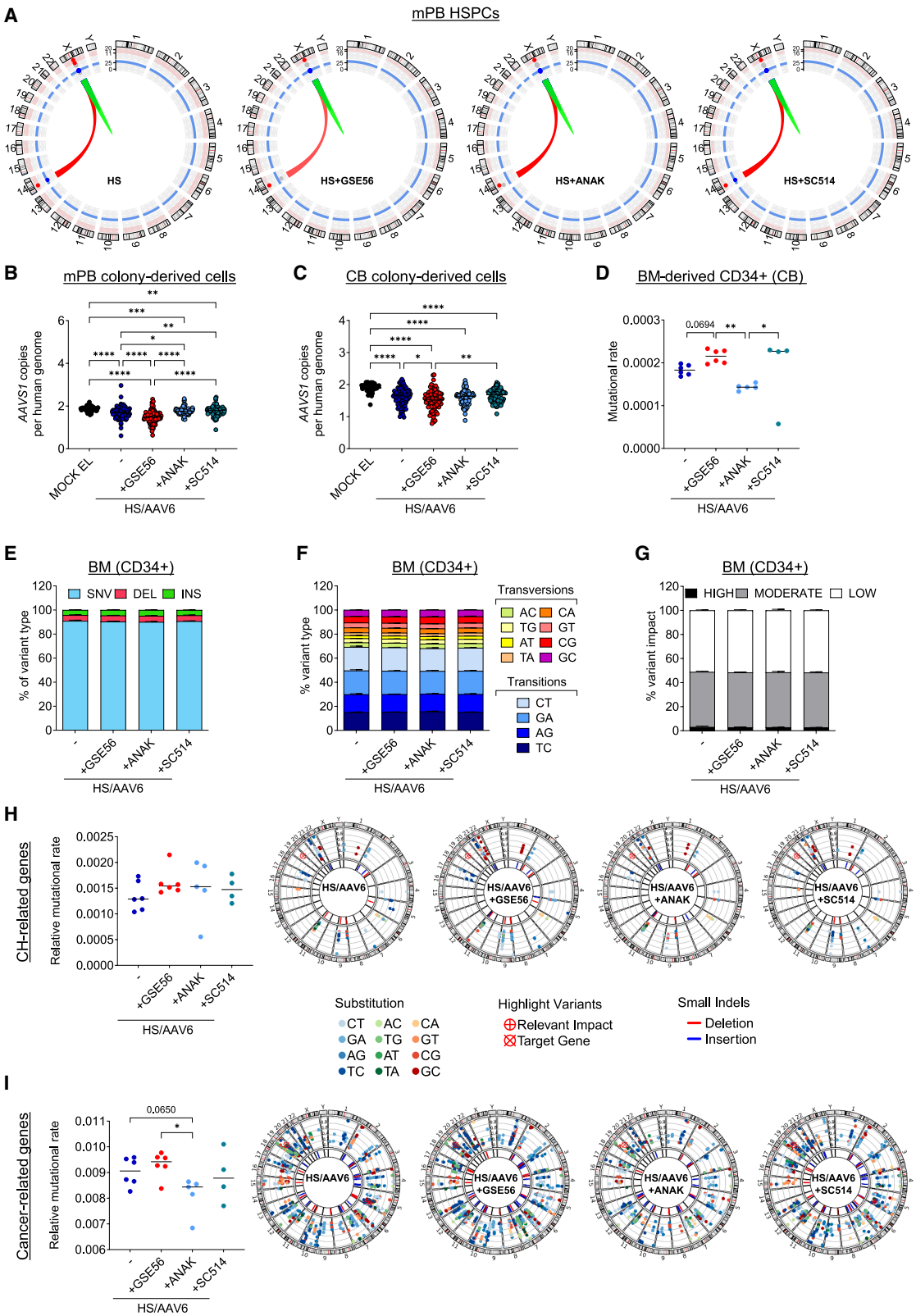
(M) Percentage of SA-β-Gal$^+$ cells in BM of mice shown in (I) at 15 weeks post-transplantation; Kruskal-Wallis test.

(N) Number of colonies grown from BM-derived CD34$^+$ HSPCs of mice shown in (I) 15 weeks post-transplantation (n = 6, 6, 6, 6, and 5); Kruskal-Wallis test; mean ± SEM.

(O) Number of unique indels in human BM-derived cells of mice transplanted with CB HSPCs from (A) (n = 13, 12, 12, and 12 from 3 independent *in vivo* experiments); Kruskal-Wallis test.

(P) Number of dominant unique BARs in BM-derived cells of mice transplanted with CB HSPCs in (A) (n = 19, 15, 19, and 12 from 4 independent *in vivo* experiments); Kruskal-Wallis test.

p values: *$p < 0.05$; **$p < 0.01$; ***$p < 0.001$; ****$p < 0.0001$. If not indicated, results are not significant (ns). Unless otherwise specified, lines indicate median values. (–): HS/AAV6 condition.



(legend on next page)

Limitations of the study

While promising, our findings have limitations. We cannot rule out that optimizing HSPC culture conditions during GE, such as reducing pro-inflammatory cytokines and growth factors or refining AAV6 vector[64] doses and purity, could reduce the senescence burden observed *ex vivo* and *in vivo*. Further evaluation of anti-inflammatory treatments in disease models will strengthen the rationale for clinical application of our protocol. Lastly, exploring alternative GE platforms, such as base and prime editors or transposases will provide broader understanding of the relationship between GE strategies and cellular senescence.

RESOURCE AVAILABILITY

Lead contact

The lead contact for this work is Raffaella Di Micco (dimicco.raffaella@hsr.it).

Materials availability

This study did not generate new reagents.

Data and code availability

- The RNA-seq data have been deposited in NCBI's Gene Expression Omnibus and are accessible through GEO SuperSeries accession number GSE244257. The SuperSeries contains the following SubSeries:
  - GSE244247 (RNA-seq DAY1)
  - GSE244248 (RNA-seq DAY4)
  - GSE287803 (BAR-seq)
  - GSE287805 (NHEJ-seq)
- WES data are deposited at the European Nucleotide Archive (accession number: PRJEB66213).
- The code used for the analysis is available at the GitLab repository: http://www.bioinfotiget.it/gitlab/custom/conti_ge_2025.
- Additional data for reanalysis are available from the lead contact upon request.

ACKNOWLEDGMENTS

We thank G. Andrieux for bioinformatic analysis of CAST-Seq data, M.Fiumara for GSE56 mRNA production, C. Gaddoni for technical help on translocations analysis, D. Canarutto for developing assays for detection of large deletions, A. Anselmo for technical support with SPiDER-β-Gal staining, C. Di Serio for coordinating Centro Universitario di Statistica per le Scienze Biomediche (CUSSB), and the FRACTAL and ALEMBIC facilities at San Raffaele Hospital. The illustrations were created with BioRender.com. F.M., L.A., A.W., D.G. and L.d.V. conducted this study partially fulfilling their Ph.D. in Molecular Medicine, Vita-Salute San Raffaele University. A.V. is supported by a Boehringer Ingelheim Fonds PhD fellowship. S.Z.X. is supported by The Princess Margaret Cancer Foundation. Research in R.D. Micco lab is supported by My First AIRC Grant (MFAG 2019–PI ID.23321), Fondazione Telethon (Tele21-E5), Career Development Award from Human Frontier Science Program, New York Stem Cell Foundation, European Research Council (consolidator grant 101003186, ReviveSTEM), and Horizon Europe 2020 Program X-PAND grant (G.A. 101070950). Work in the labs of L.N. and T.C. was supported by Horizon Europe 2020 Program UPGRADE (to L.N.) and X-PAND (to L.N. and T.C.) grant (G.A. 101070950). P.Z. is a scholarship recipient of the German Academic Exchange Service (DAAD 91764871). A.C. is an EHA-ASH TRTH investigator. R.D. Micco is a New York Stem Cell Foundation Robertson Investigator.

AUTHOR CONTRIBUTIONS

A.C. planned, performed, and coordinated research; supervised R.D. Marco; analyzed and interpreted data; and wrote the manuscript. I.M. coordinated the bioinformatic analyses performed by S.B., T.T., and N.G. R.D. Marco performed senescence stainings and micronuclei quantification. F.M. contributed to GE experiments *in vivo*, discussed the results, and wrote the manuscript. A.V. performed large DEL analysis supervised by S. Z.X. P.Z. performed CAST-Seq under the supervision of T.C. S.F. performed clonal tracking analysis, discussed the results, and edited the manuscript. A.W. helped with translocation analysis. L.N. supervised S.F. and A.W. and edited the manuscript. C.B. performed LME statistical analysis. D.G., L.d.V., K.G., and E.C. provided technical help for animal experiments. K.G. discussed data and wrote the manuscript. R.D. Micco conceived the study, interpreted data, coordinated research, supervised all team members, secured funding, and wrote the manuscript.

DECLARATION OF INTERESTS

R.D. Micco, A.C., L.d.V., F.M., L.N., and S.F. are inventors of patents on applications of gene editing in HSPCs owned and managed by the San Raffaele Scientific Institute and the Telethon Foundation. L.N. is a founder and quota holder of Genespire. T.C. is an inventor of patents on the applications of CAST-Seq.

STAR★METHODS

Detailed methods are provided in the online version of this paper and include the following:

- KEY RESOURCES TABLE
- EXPERIMENTAL MODEL AND STUDY PARTICIPANT DETAILS
  - Mice
  - Primary cell cultures
- METHOD DETAILS
  - Gene editing of human HSPCs
  - p53 inhibition and anti-inflammatory treatments
  - Gene editing efficiency analyses
  - Digital droplet PCR (ddPCR)
  - NHEJ analysis

Figure 7. Anakinra treatment reduces the genotoxicity risk associated with the gene-editing procedure

(A) Visualization of chromosomal translocation genome wide by CAST-Seq.[45]

(B and C) Copies of *AAVS1* sequences per human genome 800 bp downstream to the target site in individual colonies generated by edited mPB HSPCs (B: $n = 46$, 93, 97, 93, and 85) or CB HSPCs (C: $n = 48$, 91, 92, 98, and 97) from 3 independent donors. LME, linear-mixed model.

(D) Mutational rate of total variants in the indicated conditions from BM-derived CD34$^+$ HSPCs of mice from one independent experiment from Figure S6I ($n = 6, 6, 5$, and 4); Kruskal-Wallis test.

(E) Percentage of single-nucleotide variants (SNVs), deletions (DELs), and insertions (INSs) in BM-derived CD34$^+$ HSPCs retrieved from mice in (D). $n = 6, 6, 5$, and 4; Kruskal-Wallis test; mean ± SEM.

(F) Relative proportion (percentages) of SNV types in mice in (E). $n = 6, 6, 5$, and 4; Kruskal-Wallis test; mean ± SEM.

(G) Percentage of variants with high (HIGH), moderate (MODERATE), or low (LOW) impact found in BM-derived CD34$^+$ HSPCs retrieved from mice in (D) ($n = 6, 6, 5$, and 4); Kruskal-Wallis test; mean ± SEM.

(H and I) Quantification and Circos plots representing variants in clonal hematopoiesis (CH)-associated genes (H) or cancer-associated genes (I) ($n = 6, 6, 5$, and 4); Kruskal-Wallis test.

p values: $^*p < 0.05$; $^{**}p < 0.01$; $^{***}p < 0.001$; $^{****}p < 0.0001$. If not indicated, results are not significant (ns). Unless otherwise specified, lines indicate median values. (–): HS/AAV6 condition.

- Colony-forming unit (CFU-C) cell assay
- Gene expression analysis by RT quantitative PCR (RT q-PCR)
- $CD34^+$ HSPC xenotransplantation studies in NSG mice
- Flow cytometry
- Fluorescent senescence-associated-β-galactosidase staining with SPiDER-β-Gal and CDKN2A (p16) intracellular staining
- Immunofluorescence analysis
- BAR-seq library preparation
- BAR-seq analyses
- Indels-based clonal tracking library preparation
- Indels-based clonal tracking analysis
- Total RNA-Seq library preparation
- Bulk and single-cell RNA-seq analyses
- Analysis of large deletions at the edited site
- Translocation analysis on colonies derived from HSPCs
- CAST-seq
- Whole exome sequencing sample preparation and analysis

- QUANTIFICATION AND STATISTICAL ANALYSIS

SUPPLEMENTAL INFORMATION

Supplemental information can be found online at https://doi.org/10.1016/j.xcrm.2025.102157.

Received: October 9, 2023
Revised: February 28, 2025
Accepted: May 6, 2025
Published: June 3, 2025

REFERENCES

1. Ferrari, S., Valeri, E., Conti, A., Scala, S., Aprile, A., Di Micco, R., Kajaste-Rudnitski, A., Montini, E., Ferrari, G., Aiuti, A., and Naldini, L. (2023). Genetic engineering meets hematopoietic stem cell biology for next-generation gene therapy. Cell Stem Cell *30*, 549–570. https://doi.org/10.1016/J.STEM.2023.04.014.
2. Doudna, J.A., and Charpentier, E. (2014). The new frontier of genome engineering with CRISPR-Cas9 at American Association for the Advancement of Science. Science *28*, 1258096. https://doi.org/10.1126/science.1258096.
3. Porteus, M.H. (2019). A New Class of Medicines through DNA Editing. N. Engl. J. Med. *380*, 947–959.
4. Kohn, D.B., Chen, Y.Y., and Spencer, M.J. (2023). Successes and challenges in clinical gene therapy. Gene Ther. *30*, 738–746. https://doi.org/10.1038/S41434-023-00390-5.
5. Salsman, J., and Dellaire, G. (2017). Precision genome editing in the CRISPR era. Biochem. Cell. Biol. *95*, 187–201. https://doi.org/10.1139/BCB-2016-0137.
6. Azhagiri, M.K.K., Babu, P., Venkatesan, V., and Thangavel, S. (2021). Homology-directed gene-editing approaches for hematopoietic stem and progenitor cell gene therapy. Stem Cell Res. Ther. *12*, 500. https://doi.org/10.1186/S13287-021-02565-6.
7. Wienert, B., Nguyen, D.N., Guenther, A., Feng, S.J., Locke, M.N., Wyman, S.K., Shin, J., Kazane, K.R., Gregory, G.L., Carter, M.A.M., et al. (2020). Timed inhibition of CDC7 increases CRISPR-Cas9 mediated templated repair. Nat. Commun. *11*, 2109–2115. https://doi.org/10.1038/s41467-020-15845-1.
8. Genovese, P., Schiroli, G., Escobar, G., Tomaso, T.D., Firrito, C., Calabria, A., Moi, D., Mazzieri, R., Bonini, C., Holmes, M.C., et al. (2014). Targeted genome editing in human repopulating haematopoietic stem cells. Nature *510*, 235–240. https://doi.org/10.1038/nature13420.
9. Ferrari, S., Jacob, A., Cesana, D., Laugel, M., Beretta, S., Varesi, A., Unali, G., Conti, A., Canarutto, D., Albano, L., et al. (2022). Choice of template delivery mitigates the genotoxic risk and adverse impact of editing in human hematopoietic stem cells. Cell Stem Cell *29*, 1428–1444.e9. https://doi.org/10.1016/J.STEM.2022.09.001.
10. Wang, J., Exline, C.M., Declercq, J.J., Llewellyn, G.N., Hayward, S.B., Li, P.W.L., Shivak, D.A., Surosky, R.T., Gregory, P.D., Holmes, M.C., and Cannon, P.M. (2015). Homology-driven genome editing in hematopoietic stem and progenitor cells using ZFN mRNA and AAV6 donors. Nat. Biotechnol. *33*, 1256–1263. https://doi.org/10.1038/nbt.3408.
11. Salisbury-Ruf, C.T., and Larochelle, A. (2021). Advances and Obstacles in Homology-Mediated Gene Editing of Hematopoietic. J. Clin. Med. *10*, 513. https://doi.org/10.3390/JCM10030513.
12. Charlesworth, C.T., Camarena, J., Cromer, M.K., Vaidyanathan, S., Bak, R.O., Carte, J.M., Potter, J., Dever, D.P., and Porteus, M.H. (2018). Priming Human Repopulating Hematopoietic Stem and Progenitor Cells for Cas9/sgRNA Gene Targeting. Mol. Ther. Nucleic Acids *12*, 89–104. https://doi.org/10.1016/J.OMTN.2018.04.017.
13. Lattanzi, A., Camarena, J., Lahiri, P., Segal, H., Srifa, W., Vakulskas, C.A., Frock, R.L., Kenrick, J., Lee, C., Talbott, N., et al. (2021). Development of β-globin gene correction in human hematopoietic stem cells as a potential durable treatment for sickle cell disease. Sci. Transl. Med. *13*, eabf2444. https://doi.org/10.1126/SCITRANSLMED.ABF2444.
14. Schiroli, G., Conti, A., Ferrari, S., della Volpe, L., Jacob, A., Albano, L., Beretta, S., Calabria, A., Vavassori, V., Gasparini, P., et al. (2019). Precise Gene Editing Preserves Hematopoietic Stem Cell Function following Transient p53-Mediated DNA Damage Response. Cell Stem Cell *24*, 551–565.e8. https://doi.org/10.1016/j.stem.2019.02.019.
15. della Volpe, L., Midena, F., Vacca, R., Tavella, T., Alessandrini, L., Farina, G., Brandas, C., Lo Furno, E., Giannetti, K., Carsana, E., et al. (2024). A p38 MAPK-ROS axis fuels proliferation stress and DNA damage during CRISPR-Cas9 gene editing in hematopoietic stem and progenitor cells. Cell Rep. Med. *5*, 101823. https://doi.org/10.1016/J.XCRM.2024.101823.
16. Rai, R., Naseem, A., Vetharoy, W., Steinberg, Z., Thrasher, A.J., Santilli, G., and Cavazza, A. (2023). An improved medium formulation for efficient ex vivo gene editing, expansion and engraftment of hematopoietic stem and progenitor cells. Mol. Ther. Methods Clin. Dev. *29*, 58–69. https://doi.org/10.1016/J.OMTM.2023.02.014.
17. Ferrari, S., Jacob, A., Beretta, S., Unali, G., Albano, L., Vavassori, V., Cittaro, D., Lazarevic, D., Brombin, C., Cugnata, F., et al. (2020). Efficient gene editing of human long-term hematopoietic stem cells validated by clonal tracking. Nat. Biotechnol. *38*, 1298–1308. https://doi.org/10.1038/s41587-020-0551-y.
18. Lomova, A., Clark, D.N., Campo-Fernandez, B., Flores-Bjurström, C., Kaufman, M.L., Fitz-Gibbon, S., Wang, X., Miyahira, E.Y., Brown, D., DeWitt, M.A., et al. (2019). Improving Gene Editing Outcomes in Human Hematopoietic Stem and Progenitor Cells by Temporal Control of DNA Repair. Stem Cell. *37*, 284–294. https://doi.org/10.1002/stem.2935.
19. Shin, J.J., Schröder, M.S., Caiado, F., Wyman, S.K., Bray, N.L., Bordi, M., Dewitt, M.A., Vu, J.T., Kim, W.T., Hockemeyer, D., et al. (2020). Controlled Cycling and Quiescence Enables Efficient HDR in Engraftment-Enriched Adult Hematopoietic Stem and Progenitor Cells. Cell Rep. *32*, 108093. https://doi.org/10.1016/j.celrep.2020.108093.
20. Canny, M.D., Moatti, N., Wan, L.C.K., Fradet-Turcotte, A., Krasner, D., Mateos-Gomez, P.A., Zimmermann, M., Orthwein, A., Juang, Y.C., Zhang, W., et al. (2018). Inhibition of 53BP1 favors homology-dependent DNA repair and increases CRISPR-Cas9 genome-editing efficiency. Nat. Biotechnol. *36*, 95–102. https://doi.org/10.1038/nbt.4021.
21. De Ravin, S.S., Li, L., Wu, X., Choi, U., Allen, C., Koontz, S., Lee, J., Theobald-Whiting, N., Chu, J., Garofalo, M., et al. (2017). CRISPR-Cas9 gene repair of hematopoietic stem cells from patients with X-linked chronic granulomatous disease. Sci. Transl. Med. *9*, eaah3480. https://doi.org/10.1126/scitranslmed.aah3480.
22. Pattabhi, S., Lotti, S.N., Berger, M.P., Singh, S., Lux, C.T., Jacoby, K., Lee, C., Negre, O., Scharenberg, A.M., and Rawlings, D.J. (2019). In Vivo Outcome of Homology-Directed Repair at the HBB Gene in HSC Using

Alternative Donor Template Delivery Methods. Mol. Ther. Nucleic Acids *17*, 277–288. https://doi.org/10.1016/j.omtn.2019.05.025.

23. Romero, Z., Lomova, A., Said, S., Miggelbrink, A., Kuo, C.Y., Campo-Fernandez, B., Hoban, M.D., Masiuk, K.E., Clark, D.N., Long, J., et al. (2019). Editing the Sickle Cell Disease Mutation in Human Hematopoietic Stem Cells: Comparison of Endonucleases and Homologous Donor Templates. Mol. Ther. *27*, 1389–1406. https://doi.org/10.1016/j.ymthe.2019.05.014.
24. Shy, B.R., Vykunta, V.S., Ha, A., Talbot, A., Roth, T.L., Nguyen, D.N., Pfeifer, W.G., Chen, Y.Y., Blaeschke, F., Shifrut, E., et al. (2023). High-yield genome engineering in primary cells using a hybrid ssDNA repair template and small-molecule cocktails. Nat. Biotechnol. *41*, 521–531. https://doi.org/10.1038/S41587-022-01418-8.
25. Zeng, J., Nguyen, M.A., Liu, P., da Silva, L.F., Levesque, S., Lin, L.Y., Justus, D.G., Petri, K., Clement, K., Porter, S.N., et al. (2025). Gene editing without ex vivo culture evades genotoxicity in human hematopoietic stem cells. Cell Stem Cell *32*, 191–208.e11. https://doi.org/10.1016/J.STEM.2024.11.001.
26. Kuo, C.Y., Long, J.D., Campo-Fernandez, B., de Oliveira, S., Cooper, A.R., Romero, Z., Hoban, M.D., Joglekar, A.V., Lill, G.R., Kaufman, M.L., et al. (2018). Site-Specific Gene Editing of Human Hematopoietic Stem Cells for X-Linked Hyper-IgM Syndrome. Cell Rep. *23*, 2606–2616. https://doi.org/10.1016/j.celrep.2018.04.103.
27. Piras, F., Riba, M., Petrillo, C., Lazarevic, D., Cuccovillo, I., Bartolaccini, S., Stupka, E., Gentner, B., Cittaro, D., Naldini, L., and Kajaste-Rudnitski, A. (2017). Lentiviral vectors escape innate sensing but trigger p53 in human hematopoietic stem and progenitor cells. EMBO Mol. Med. *9*, 1198–1211. https://doi.org/10.15252/emmm.201707922.
28. Baik, R., Cromer, M.K., Glenn, S.E., Vakulskas, C.A., Chmielewski, K.O., Dudek, A.M., Feist, W.N., Klermund, J., Shipp, S., Cathomen, T., et al. (2024). Transient inhibition of 53BP1 increases the frequency of targeted integration in human hematopoietic stem and progenitor cells. Nat. Commun. *15*, 111–114. https://doi.org/10.1038/s41467-023-43413-w.
29. Cullot, G., Aird, E.J., Schlapansky, M.F., Yeh, C.D., van de Venn, L., Vykhlyantseva, I., Kreutzer, S., Mailänder, D., Lewków, B., Klermund, J., et al. (2024). Genome editing with the HDR-enhancing DNA-PKcs inhibitor AZD7648 causes large-scale genomic alterations. Nat. Biotechnol., 1–5. https://doi.org/10.1038/s41587-024-02488-6.
30. Di Micco, R., Krizhanovsky, V., Baker, D., and d'Adda di Fagagna, F. (2021). Cellular senescence in ageing: from mechanisms to therapeutic opportunities. Nat Rev Mol Cell Biol. *22*, 75–95.
31. Biavasco, R., Lettera, E., Giannetti, K., Gilioli, D., Beretta, S., Conti, A., Scala, S., Cesana, D., Gallina, P., Norelli, M., et al. (2021). Oncogene-induced senescence in hematopoietic progenitors features myeloid restricted hematopoiesis, chronic inflammation and histiocytosis. Nat. Commun. *12*, 4559. https://doi.org/10.1038/S41467-021-24876-1.
32. Cinat, D., Coppes, R.P., and Barazzuol, L. (2021). DNA Damage-Induced Inflammatory Microenvironment and Adult Stem Cell Response. Front. Cell Dev. Biol. *9*, 729136. https://doi.org/10.3389/FCELL.2021.729136/BIBTEX.
33. Rodier, F., Coppé, J.P., Patil, C.K., Hoeijmakers, W.A.M., Muñoz, D.P., Raza, S.R., Freund, A., Campeau, E., Davalos, A.R., and Campisi, J. (2009). Persistent DNA damage signalling triggers senescence-associated inflammatory cytokine secretion. Nat. Cell Biol. *11*, 973–979. https://doi.org/10.1038/ncb1909.
34. Purcell, M., Kruger, A., and Tainsky, M.A. (2014). Gene expression profiling of replicative and induced senescence. Cell Cycle *13*, 3927–3937. https://doi.org/10.4161/15384101.2014.973327.
35. Pribluda, A., Elyada, E., Wiener, Z., Hamza, H., Goldstein, R.E., Biton, M., Burstain, I., Morgenstern, Y., Brachya, G., Billauer, H., et al. (2013). A senescence-inflammatory switch from cancer-inhibitory to cancer-promoting mechanism. Cancer Cell *24*, 242–256. https://doi.org/10.1016/J.CCR.2013.06.005.
36. Saul, D., Kosinsky, R.L., Atkinson, E.J., Doolittle, M.L., Zhang, X., LeBrasseur, N.K., Pignolo, R.J., Robbins, P.D., Niedernhofer, L.J., Ikeno, Y., et al. (2022). A new gene set identifies senescent cells and predicts senescence-associated pathways across tissues. Nat. Commun. *13*, 4827. https://doi.org/10.1038/S41467-022-32552-1.
37. Jochems, F., Thijssen, B., De Conti, G., Jansen, R., Pogacar, Z., Groot, K., Wang, L., Schepers, A., Wang, C., Jin, H., et al. (2021). The Cancer SENESCopedia: A delineation of cancer cell senescence. Cell Rep. *36*, 109441. https://doi.org/10.1016/J.CELREP.2021.109441.
38. Schleich, K., Kase, J., Dörr, J.R., Trescher, S., Bhattacharya, A., Yu, Y., Wailes, E.M., Fan, D.N.Y., Lohneis, P., Milanovic, M., et al. (2020). H3K9me3-mediated epigenetic regulation of senescence in mice predicts outcome of lymphoma patients. Nat. Commun. *11*. https://doi.org/10.1038/S41467-020-17467-Z.
39. Vavassori, V., Mercuri, E., Marcovecchio, G.E., Castiello, M.C., Schiroli, G., Albano, L., Margulies, C., Buquicchio, F., Fontana, E., Beretta, S., et al. (2021). Modeling, optimization, and comparable efficacy of T cell and hematopoietic stem cell gene editing for treating hyper-IgM syndrome. EMBO Mol. Med. *13*, e13545. https://doi.org/10.15252/EMMM.202013545.
40. Cavalli, G., and Dinarello, C.A. (2018). Anakinra Therapy for Non-cancer Inflammatory Diseases. Front. Pharmacol. *9*, 1157. https://doi.org/10.3389/FPHAR.2018.01157.
41. Pietras, E.M. (2017). Inflammation: A key regulator of hematopoietic stem cell fate in health and disease. Blood *130*, 1693–1698. https://doi.org/10.1182/blood-2017-06-780882.
42. Gnani, D., Crippa, S., della Volpe, L., Rossella, V., Conti, A., Lettera, E., Rivis, S., Ometti, M., Fraschini, G., Bernardo, M.E., and Di Micco, R. (2019). An early-senescence state in aged mesenchymal stromal cells contributes to hematopoietic stem and progenitor cell clonogenic impairment through the activation of a pro-inflammatory program. Aging Cell *18*, e12933. https://doi.org/10.1111/acel.12933.
43. Chien, Y., Scuoppo, C., Wang, X., Fang, X., Balgley, B., Bolden, J.E., Premsrirut, P., Luo, W., Chicas, A., Lee, C.S., et al. (2011). Control of the senescence-associated secretory phenotype by NF-κB promotes senescence and enhances chemosensitivity. Genes Dev. *25*, 2125–2136. https://doi.org/10.1101/GAD.17276711.
44. Milyavsky, M., Gan, O.I., Trottier, M., Komosa, M., Tabach, O., Notta, F., Lechman, E., Hermans, K.G., Eppert, K., Konovalova, Z., et al. (2010). A Distinctive DNA damage response in human hematopoietic stem cells reveals an apoptosis-independent role for p53 in self-renewal. Cell Stem Cell *7*, 186–197. https://doi.org/10.1016/j.stem.2010.05.016.
45. Turchiano, G., Andrieux, G., Klermund, J., Blattner, G., Pennucci, V., el Gaz, M., Monaco, G., Poddar, S., Mussolino, C., Cornu, T.I., et al. (2021). Quantitative evaluation of chromosomal rearrangements in gene-edited human stem cells by CAST-Seq. Cell Stem Cell *28*, 1136–1147.e5.
46. Leibowitz, M.L., Papathanasiou, S., Doerfler, P.A., Blaine, L.J., Sun, L., Yao, Y., Zhang, C.Z., Weiss, M.J., and Pellman, D. (2021). Chromothripsis as an on-target consequence of CRISPR–Cas9 genome editing. Nat. Genet. *53*, 895–905. https://doi.org/10.1038/s41588-021-00838-7.
47. Ihry, R.J., Worringer, K.A., Salick, M.R., Frias, E., Ho, D., Theriault, K., Kommineni, S., Chen, J., Sondey, M., Ye, C., et al. (2018). P53 inhibits CRISPR-Cas9 engineering in human pluripotent stem cells. Nat. Med. *24*, 939–946. https://doi.org/10.1038/s41591-018-0050-6.
48. Sinha, S., Barbosa, K., Cheng, K., Leiserson, M.D.M., Jain, P., Deshpande, A., Wilson, D.M., Ryan, B.M., Luo, J., Ronai, Z.A., et al. (2021). A systematic genome-wide mapping of oncogenic mutation selection during CRISPR-Cas9 genome editing. Nat. Commun. *12*, 6512. https://doi.org/10.1038/S41467-021-26788-6.
49. Cingolani, P., Platts, A., Wang, L.L., Coon, M., Nguyen, T., Wang, L., Land, S.J., Lu, X., and Ruden, D.M. (2012). A program for annotating and predicting the effects of single nucleotide polymorphisms, SnpEff: SNPs in the genome of Drosophila melanogaster strain w1118; iso-2; iso-3. Fly (Austin) *6*, 80–92. https://doi.org/10.4161/FLY.19695.
50. Busque, L., Buscarlet, M., Mollica, L., and Levine, R.L. (2018). Concise Review: Age-Related Clonal Hematopoiesis: Stem Cells Tempting the Devil. Stem Cell. *36*, 1287–1294. https://doi.org/10.1002/STEM.2845.

51. Walter, D., Lier, A., Geiselhart, A., Thalheimer, F.B., Huntscha, S., Sobotta, M. C., Moehrle, B., Brocks, D., Bayindir, I., Kaschutnig, P., et al. (2015). Exit from dormancy provokes DNA-damage-induced attrition in haematopoietic stem cells. Nature *520*, 549–552. https://doi.org/10.1038/nature14131.

52. Jacobs, K., Doerdelmann, C., Krietsch, J., González-Acosta, D., Mathis, N., Kushinsky, S., Guarino, E., Gómez-Escolar, C., Martinez, D., Schmid, J.A., et al. (2022). Stress-triggered hematopoietic stem cell proliferation relies on PrimPol-mediated repriming. Mol. Cell *82*, 4176–4188.e8. https://doi.org/10.1016/J.MOLCEL.2022.09.009.

53. Biechonski, S., Olender, L., Zipin-Roitman, A., Yassin, M., Aqaqe, N., Marcu-Malina, V., Rall-Scharpf, M., Trottier, M., Meyn, M.S., Wiesmüller, L., et al. (2018). Attenuated DNA damage responses and increased apoptosis characterize human hematopoietic stem cells exposed to irradiation. Sci. Rep. *8*, 6071. https://doi.org/10.1038/S41598-018-24440-W.

54. Xu, M., Pirtskhalava, T., Farr, J.N., Weigand, B.M., Palmer, A.K., Weivoda, M. M., Inman, C.L., Ogrodnik, M.B., Hachfeld, C.M., Fraser, D.G., et al. (2018). Senolytics Improve Physical Function and Increase Lifespan in Old Age. Nat. Med. *24*, 1246–1256. https://doi.org/10.1038/S41591-018-0092-9.

55. Orjalo, A.V., Bhaumik, D., Gengler, B.K., Scott, G.K., and Campisi, J. (2009). Cell surface-bound IL-1α is an upstream regulator of the senescence-associated IL-6/IL-8 cytokine network. Proc. Natl. Acad. Sci. USA *106*, 17031–17036. https://doi.org/10.1073/pnas.0905299106.

56. Pietras, E.M., Mirantes-Barbeito, C., Fong, S., Loeffler, D., Kovtonyuk, L.V., Zhang, S., Lakshminarasimhan, R., Chin, C.P., Techner, J.M., Will, B., et al. (2016). Chronic interleukin-1 exposure drives haematopoietic stem cells towards precocious myeloid differentiation at the expense of self-renewal. Nat. Cell Biol. *18*, 607–618. https://doi.org/10.1038/ncb3346.

57. Kovtonyuk, L.V., Caiado, F., Garcia-Martin, S., Manz, E.M., Helbling, P., Takizawa, H., Boettcher, S., Al-Shahrour, F., Nombela-Arrieta, C., Slack, E., and Manz, M.G. (2022). IL-1 mediates microbiome-induced inflammaging of hematopoietic stem cells in mice. Blood *139*, 44–58. https://doi.org/10.1182/BLOOD.2021011570.

58. Ye, H., Qian, L., Zhu, S., Deng, S., Wang, X., Zhu, J., Chan, G.L., Yu, Y., and Han, W. (2019). IL-1Ra protects hematopoietic cells from chemotoxicity through p53-induced quiescence. FASEB J. *33*, 12135–12145. https://doi.org/10.1096/FJ.201900788RR.

59. Qian, L., Xiang, D., Zhang, J., Zhu, S., Gao, J., Wang, X., Gao, J., Zhang, Y., Shen, J., Yu, Y., et al. (2013). Recombinant human interleukin-1 receptor antagonist reduces acute lethal toxicity and protects hematopoiesis from chemotoxicity in vivo. Biomed. Pharmacother. *67*, 108–115. https://doi.org/10.1016/J.BIOPHA.2012.11.002.

60. Amendola, M., Brusson, M., and Miccio, A. (2022). CRISPRthripsis: The Risk of CRISPR/Cas9-induced Chromothripsis in Gene Therapy. Stem Cells Transl. Med. *11*, 1003–1009. https://doi.org/10.1093/STCLTM/SZAC064.

61. Jiang, Q., Isquith, J., Ladel, L., Mark, A., Holm, F., Mason, C., He, Y., Mondala, P., Oliver, I., Pham, J., et al. (2021). Inflammation-driven deaminase deregulation fuels human pre-leukemia stem cell evolution. Cell Rep. *34*, 108670. https://doi.org/10.1016/J.CELREP.2020.108670.

62. Zipeto, M.A., Court, A.C., Sadarangani, A., Delos Santos, N.P., Balaian, L., Chun, H.J., Pineda, G., Morris, S.R., Mason, C.N., Geron, I., et al. (2016). ADAR1 Activation Drives Leukemia Stem Cell Self-Renewal by Impairing Let-7 Biogenesis. Cell Stem Cell *19*, 177–191. https://doi.org/10.1016/J.STEM.2016.05.004.

63. Idan, C., Peleg, R., Elena, V., Martin, T., Cicerone, T., Mareike, W., Lydia, B., Marina, F., Gerhard, M., Elisa, F.M., et al. (2015). IL-1α is a DNA damage sensor linking genotoxic stress signaling to sterile inflammation and innate immunity. Sci. Rep. *5*. https://doi.org/10.1038/SREP14756.

64. Subramanian, A., Tamayo, P., Mootha, V.K., Mukherjee, S., Ebert, B.L., Gillette, M.A., Paulovich, A., Pomeroy, S.L., Golub, T.R., Lander, E.S., and Mesirov, J.P. (2005). Gene set enrichment analysis: a knowledge-based approach for interpreting genome-wide expression profiles. Proc. Natl. Acad. Sci. USA *102*, 15545–15550. https://doi.org/10.1073/PNAS.0506580102.

65. Clement, K., Rees, H., Canver, M.C., Gehrke, J.M., Farouni, R., Hsu, J.Y., Cole, M.A., Liu, D.R., Joung, J.K., Bauer, D.E., et al. (2019). CRISPResso2 provides accurate and rapid genome editing sequence analysis. Nat Biotechnol. *37*, 224–226.

66. Strobel, B., Miller, F.D., Rist, W., and Lamla, T. (2015). Comparative Analysis of Cesium Chloride- and Iodixanol-Based Purification of Recombinant Adeno-Associated Viral Vectors for Preclinical Applications. Hum. Gene Ther. Methods *26*, 147–157. https://doi.org/10.1089/HGTB.2015.051.

67. Schiroli, G., Ferrari, S., Conway, A., Jacob, A., Capo, V., Albano, L., Plati, T., Castiello, M.C., Sanvito, F., Gennery, A.R., et al. (2017). Preclinical modeling highlights the therapeutic potential of hematopoietic stem cell gene editing for correction of SCID-X1. Sci. Transl. Med. *9*, eaan0820. https://doi.org/10.1126/scitranslmed.aan0820.

68. Doura, T., Kamiya, M., Obata, F., Yamaguchi, Y., Hiyama, T.Y., Matsuda, T., Fukamizu, A., Noda, M., Miura, M., and Urano, Y. (2016). Detection of LacZ-Positive Cells in Living Tissue with Single-Cell Resolution. Angew. Chem. Int. Ed. Engl. *55*, 9620–9624. https://doi.org/10.1002/ANIE.201603328.

69. Moiseeva, V., Cisneros, A., Sica, V., Deryagin, O., Lai, Y., Jung, S., Andrés, E., An, J., Segalés, J., Ortet, L., et al. (2023). Senescence atlas reveals an aged-like inflamed niche that blunts muscle regeneration. Nature *613*, 169–178. https://doi.org/10.1038/S41586-022-05535-X.

70. Lassmann, T. (2015). TagDust2: A generic method to extract reads from sequencing data. BMC Bioinf. *16*, 24. https://doi.org/10.1186/s12859-015-0454-y.

71. Dobin, A., Davis, C.A., Schlesinger, F., Drenkow, J., Zaleski, C., Jha, S., Batut, P., Chaisson, M., and Gingeras, T.R. (2013). STAR: ultrafast universal RNA-seq aligner. Bioinformatics *29*, 15–21. https://doi.org/10.1093/BIOINFORMATICS/BTS635.

72. Liao, Y., Smyth, G.K., and Shi, W. (2014). featureCounts: an efficient general purpose program for assigning sequence reads to genomic features. Bioinformatics *30*, 923–930. https://doi.org/10.1093/BIOINFORMATICS/BTT656.

73. Love, M.I., Huber, W., and Anders, S. (2014). Moderated estimation of fold change and dispersion for RNA-seq data with DESeq2. Genome Biol. *15*, 550. https://doi.org/10.1186/S13059-014-0550-8.

74. Fridman, A.L., and Tainsky, M.A. (2008). Critical pathways in cellular senescence and immortalization revealed by gene expression profiling. Oncogene *27*, 5975–5987. https://doi.org/10.1038/ONC.2008.213.

75. Casella, G., Munk, R., Kim, K.M., Piao, Y., De, S., Abdelmohsen, K., and Gorospe, M. (2019). Transcriptome signature of cellular senescence. Nucleic Acids Res. *47*, 7294–7305. https://doi.org/10.1093/NAR/GKZ555.

76. Hernandez-Segura, A., de Jong, T.V., Melov, S., Guryev, V., Campisi, J., and Demaria, M. (2017). Unmasking Transcriptional Heterogeneity in Senescent Cells. Curr. Biol. *27*, 2652–2660.e4. https://doi.org/10.1016/J.CUB.2017.07.033.

77. Rhiel, M., Geiger, K., Andrieux, G., Rositzka, J., Boerries, M., Cathomen, T., and Cornu, T.I. (2023). T-CAST: An optimized CAST-Seq pipeline for TALEN confirms superior safety and efficacy of obligate-heterodimeric scaffolds. Front. Genome Ed. *5*, 1130736. https://doi.org/10.3389/FGEED.2023.1130736.

78. Klermund, J., Rhiel, M., Kocher, T., Chmielewski, K.O., Bischof, J., Andrieux, G., el Gaz, M., Hainzl, S., Boerries, M., Cornu, T.I., et al. (2024). On- and off-target effects of paired CRISPR-Cas nickase in primary human cells. Mol. Ther. *32*, 1298–1310. https://doi.org/10.1016/J.YMTHE.2024.03.006.

79. Ahdesmäki, M.J., Gray, S.R., Johnson, J.H., and Lai, Z. (2016). Disambiguate: An open-source application for disambiguating two species in next generation sequencing data from grafted samples. F1000Res. *5*, 2741. https://doi.org/10.12688/F1000RESEARCH.10082.2.

STAR★METHODS

KEY RESOURCES TABLE

REAGENT or RESOURCE	SOURCE	IDENTIFIER
Antibodies		
Anti-human CD133/1 PE-Vio 770 (Clone AC133)	Miltenyi Biotec	Cat#130-113-110; RRID: AB_2725939
Anti-human CD34 PE (Clone AC136)	Miltenyi Biotec	Cat#130-113-179; RRID: AB_2726006
Anti-human CD90 APC (Clone 5E10)	BD Biosciences	Cat#559869; RRID: AB_398677
Anti-human CD45 APC-eFluor 780 (Clone HI30)	Invitrogen	Cat#47-0459-42; RRID: AB_1944368
Anti-human CD19 PE (Clone SJ25C1)	BD Biosciences	Cat#345789; RRID: AB_2868815
Anti-human CD13 BV421 (Clone WM15)	BD Biosciences	Cat#562596; RRID: AB_2737672
Anti-human CD3 APC (Clone UCHT1)	BD Biosciences	Cat#555335; RRID: AB_398591
Anti-human CD33 PE-Cy7 (Clone P67.6)	BD Biosciences	Cat#333952; RRID: AB_2713932
Anti-human CD8 PE-Cy7 (Clone RPA-T8)	BD Biosciences	Cat#557746; RRID: AB_396852
Anti-human CD38 PerCP-Cy5.5 (Clone HB-7)	BioLegend	Cat#356614; RRID: AB_2562183
Anti-human CD34 PE-Cy7 (Clone 8G12)	BD Biosciences	Cat#348811; RRID: AB_2868855
Anti-human CD33 BV421 (Clone WM53)	BD Biosciences	Cat#562854; RRID: AB_2737405
Anti-human CD19 BV510 (Clone HIB19)	BioLegend	Cat#302242; RRID: AB_2561668
Anti-human FCR Blocking	Miltenyi Biotec	Cat#130059901; RRID: AB_2892112
Purified Rat anti-mouse CD16/CD32 (Clone 2.4G2)	BD Biosciences	Cat#553141; RRID: AB_394656
Donkey anti-Mouse IgG (H + L) Secondary Antibody, Alexa Fluor 647	Thermo Fisher Scientific	Cat#A-31571; RRID: AB_162542
Donkey anti-Rabbit IgG (H + L) Highly Cross-Absorbed Secondary Antibody, Alexa Fluor 647	Thermo Fisher Scientific	Cat#A-31573; RRID: AB_2536183
Donkey anti-Rabbit IgG (H + L) Secondary Antibody, Alexa Fluor 568	Thermo Fisher Scientific	Cat#A-10042; RRID: AB_2534017
Mouse anti-human Phospho-Histone H2A.X (Ser139) (Clone JBW301)	Merck Millipore	Cat#05-636; RRID: AB_309864
Rabbit anti-human 53BP1	Bethyl Laboratories	Cat#A300-272A; RRID: AB_185520
NFKB Tot (anti NFKB p65 (D14E12) XP	Cell Signaling Technology	Cat#8242S; RRID: AB_10859369
P16 INK4A (D7C1M) Rabbit mAb	Cell Signaling Technology	Cat#80772S; RRID:AB_2799960
Biological samples		
Umbilical cord blood	San Raffaele Hospital	N/A
Mobilized peripheral blood	Mobilized Leukopak (AllCells)	N/A
Chemicals, peptides, and recombinant proteins		
16,16-Dimethyl Prostaglandin E2	Cayman Chemical	Cat#14750
Recombinant human stem cell factor (SCF)	Peprotech	Cat#300-07
Recombinant human thrombopoietin (TPO)	Peprotech	Cat#300-18
Recombinant human Flt3-Ligand	Peprotech	Cat#300-19
Recombinant human IL6	Peprotech	Cat#200-06
StemRegenin 1 (SR1)	Biovision	Cat#1967
UM171	STEMCell Technologies	Cat#72914
Alt-R_ Cas9 Electroporation Enhancer	Integrated DNA Technologies	Cat#1075916
Alt-R CRISPR-Cas9 tracrRNA	Integrated DNA Technologies	Cat#1072534
Alt-R CRISPR-Cas9 crRNA	Integrated DNA Technologies	http://www.idtdna.com/
Alt-R CRISPR-Cas9 Negative Control crRNA #1	Integrated DNA Technologies	Cat#1072544
SpCas9 Nuclease	Aldevron	Cat#9212

(*Continued on next page*)

Continued

REAGENT or RESOURCE	SOURCE	IDENTIFIER
7-AAD Viability Staining solution	Biolegend	Cat#420403
Pacific Blue Annexin V	Biolegend	Cat#640918
Anakinra (Kineret)	SOBI	Cat#1001-119
InSolutionTM IKK-2 Inhibitor SC514	Merck	Cat#401485
SPiDER-βGal	Dojindo	Cat#SG02
Dimethyl sulfoxide (DMSO)	Sigma-Aldrich	Cat#D4818
SPHERO Rainbow Calibration Particles (8 peaks)	Spherotech	Cat#RCP305A
StemSpan SFEM	STEMCELL Technologies	Cat#09650
MethoCult H4434	STEMCELL Technologies	Cat#H4434
DAPI for nucleic acid staining	Sigma-Aldrich	Cat#D9542
Poly-L-lysine solution	Sigma-Aldrich	Cat#P8920; CAS: 25988-63-0
Paraformaldehyde solution 4% in PBS	Santa Cruz Biotechnology	Cat#SC-281692
Chloroquine diphosphate salt, solid, ≥98%	Sigma-Aldrich	Cat#C6628
CD34 MicroBead Kit, human	Miltenyi Biotec	Cat# 130-046-702
Iscove's DMEM, 1X	Corning	Cat# 15-016-CVR
Fetal Bovine Serum South America Origin	EuroClone	Cat# FA30WS1810500
Penicillin-Streptomycin (Pen-Strep) (Pen 10.000 U/mL; Strep 10.000 mg/mL)	Lonza	Cat# 17-602E
L-Glutamine 200mM	EuroClone	Cat# ECB3000D
AAVS1 gRNA (high specificity, HS)	Schiroli et al.[14]	N/A
AAVS1 gRNA (low specificity, LS)	Schiroli et al.[14]	N/A
IL2RG gRNA	Schiroli et al.[14]	N/A
Critical commercial assays		
QIAamp DNA Micro Kit	QIAGEN	Cat#56304
miRNeasy Micro Kit	QIAGEN	Cat#1071023
RNase-free DNase Set	QIAGEN	Cat#79254
iScript cDNA Synthesis Kit	Bio-Rad	Cat#170-8891
P3 Primary Cell 4D-Nucleofector X Kit S	Lonza	Cat#V4XP-3032
Fast SYBR Green Master Mix 2X	Thermo Fisher	Cat#4385618
T7 Endonuclease I	New England Biolabs	Cat#M0302L
TaqMan PreAmp Master Mix 2X	Thermo Fisher	Cat#4488593
GoTaq G2 DNA Polymerase	Promega	Cat# M7841
MinElute PCR Purification kit	QIAGEN	Cat#28004
QuickExtract DNA Extraction Solution	Lucigen	Cat#QE09050
DNeasy Blood & Tissue kit	Qiagen	Cat#69504
QIAquick PCR Purification kit	Qiagen	Cat#28104
NEBNext® Ultra™ II FS DNA Library Prep Kit for Illumina	New England Biolabs	Cat#E7805L
Deposited data		
Raw and analyzed sequencing data	This paper	GEO SuperSeries: GSE244257
RNA-seq DAY1	This paper	SubSeries: GSE244247
RNA-seq DAY4	This paper	SubSeries: GSE244248
BAR-seq	This paper	SubSeries: GSE287803
NHEJ-seq	This paper	SubSeries: GSE287805
WES	This paper	PRJEB66213
Experimental models: Cell lines		
Human cord blood $CD34^+$ Stem/Progenitor cells	Lonza	Cat#2C-101

(*Continued on next page*)

Continued		
REAGENT or RESOURCE	SOURCE	IDENTIFIER
G-CSF or G-CSF + Plerixafor mPB CD34$^+$ HSPCs	In house purification	N/A
Experimental models: Organisms/strains		
NOD.CG- PrkdcscidIl2rgtm1Wjl/SzJ (NSG) Mus Musculus	Charles River Laboratories (IACUC: #1165)	Cat# ARC:NSG, RRID:IMSR_ARC:NSG
Oligonucleotides		
See Table S1	This paper	N/A
Recombinant DNA		
pAAV2/6.PGK.GFP.BGHpa (AAVS1 HA)	Schiroli et al.[14]	N/A
pAAV2/6.PGK.GFP.bar (AAVS1 HA)	Ferrari et al.[17]	N/A
pAAV2/6.coIL2RG.PGK.GFP.BGHpa (IL2RG HA)	Schiroli et al.[14]	N/A
pAAV2/6.PGK.ΔNGFR (AAVS1 HA)	This paper	N/A
ssODN_IL2RG	Schiroli et al.[14]	N/A
pVax.GSE56.WPRE	Schiroli et al.[14]	N/A
Software and algorithms		
BD FACSDiva software	BD Biosciences	https://www.bdbiosciences.com/en-us/products/software/instrumentsoftware/
GraphPad Prism software (v.10.0.2)	GraphPad Prism	https://www.graphpad.com/
QuantaSoft (v1.7)	Bio-Rad	https://www.bio-rad.com/
ImageJ (v2.9)	NIH	https://imagej.nih.gov/ij/
FlowJo (v. 10.8.1)	FlowJo	https://www.flowjo.com/
LAS X Leica Software	Leica Mycrosystems	https://www.leica-microsystems.com/it/prodotti/software-per-microscopi/dettagli/product/leica-las-x-ls/
QuantaSoft	Bio-Rad	https://www.bio-rad.com/
QuantStudio Real-Time PCR (qPCR) software (v.1.1)	Applied Biosystems	https://www.thermofisher.com/us/en/home.html
TapeStation software	Agilent Technologies	https://www.agilent.com/en/product/automatedelectrophoresis/tapestation-systems/tapestationsoftware/tapestation-software-379381
CRISPResso2 (v2.2.8)	Clement et al.[65]	http://crispresso.pinellolab.org/submission
R statistical software (version 4.4.1)	R statistical software	https://cran.r-project.org/index.html
Code used for sequencing data analysis	This paper	http://www.bioinfotiget.it/gitlab/custom/conti_ge_2025

EXPERIMENTAL MODEL AND STUDY PARTICIPANT DETAILS

Mice

NOD-SCID-IL2Rg$^{-/-}$ (NSG) female mice were purchased from Charles River Laboratories and held in specific-pathogen-free (SPF) conditions. All experiments and procedures involving animals were designed and performed with the approval of the Animal Care and Use Committee of the San Raffaele Hospital and were authorized by the Italian Ministry of Health and local authorities according to Italian law (IACUC #1165). Transplantation experiments were performed in 8/10 weeks old female mice.

Primary cell cultures

CB CD34$^+$ HSPCs were either purchased frozen from Lonza or collected according to the TIGET09 protocol approved by the San Raffaele Hospital Ethical Committee and seeded at a concentration of 5×10^5 cells/ml in serum-free StemSpan SFEM medium (StemCell Technologies) supplemented with 100 IU/mL penicillin, 100 μg mL/1 streptomycin, 2% L-glutamine, 100 ng/mL human stem cell factor (SCF, PeproTech), 100 ng/mL human Flt3-L (PeproTech), 20 ng/mL human thrombopoietin (TPO, PeproTech),

20 ng/mL hIL-6 (PeproTech), 10 μM 16,16-dimethyl prostaglandin E2 (added at beginning of the culture; Cayman), 1 μM SR1 (Biovision) and 50 nM UM171 (StemCell Technologies). Granulocyte colony-stimulating factor (G-CSF) or G-CSF + plerixafor mobilized peripheral blood (mPB) $CD34^+$ HSPCs collected from healthy donors were purified in-house with the CliniMACS CD34 Reagent system (Miltenyi Biotec) from Mobilized Leukopak (AllCells) according to the TIGET-HPCT protocol approved by the San Raffaele Hospital Ethical Committee and following the manufacturer's instructions. HSPCs were seeded at a concentration of 5×10^5 cells per mL in serum-free StemSpan SFEM supplemented with 100 IU/mL penicillin, 100 μg/mL streptomycin, 2% L-glutamine, 300 ng/mL human stem cell factor (PreproTech), 300 ng/mL human Flt3-L (PreproTech), 100 ng/mL human thrombopoietin (PreproTech), 10 μM 16,16-dimethyl prostaglandin E2 (added at the beginning of the culture; Cayman), 1 μM SR1 (Biovision) and 35 nM UM171 (StemCell Technologies). All HSPC sources were cultured in a 20% O_2 and 5% CO_2 humidified atmosphere at 37°C.

METHOD DETAILS

Gene editing of human HSPCs

After 3 days of cytokine stimulation according to our optimized protocol,[14] cells were washed with PBS and electroporated with 25/50 pmol of Ribonucleoproteins (RNPs) using P3 Primary Cell 4D-Nucleofector X Kit and program EO-100 (Lonza) (maximum 7.5 x 10^5 cells per electroporation). RNPs were assembled by incubating Sp.Cas9 protein (Aldevron) with synthetic cr: tracrRNA (Integrated DNA Technologies) at 1:1.5 M ratio for 10–20 min at room temperature (RT, 25°C). 0.1 nmol of Alt-R Cas9 Electroporation Enhancer (Integrated DNA Technologies) was added before electroporation according to the manufacturer's instructions.[14] All HSPC transductions with AAV6 were performed at the standard dose of $1x10^4$ vg/cell within 15 min after electroporation, unless otherwise specified. Transductions with AAV6 at a dose of $2x10^3$ and $2x10^4$ vg/cell were performed where indicated. After electroporation and transduction, cells were resuspended in the culture medium and seeded at the concentration of 3×10^5 cells/ml for subsequent analyses. AAV6 donor templates for HDR were generated from a construct containing AAV2 inverted terminal repeats, produced at the TIGEM Vector Core by triple-transfection method and purified by ultracentrifugation on cesium chloride gradient, as previously described.[66] AAV6 donor templates were designed with homologies for *AAVS1* locus (encoding for a PGK.GFP or PGK.ΔLNGFF reporter cassettes) or targeting intron 1 of *IL2RG* locus (encoding for IL2RG corrective cDNA followed by a PGK.GFP reporter cassette) as previously reported.[14,67] BAR-coded AAV6 vector was provided by L. Naldini's group.[17] Where indicated, a short single-strand oligodeoxynucleotide (ssODN) was used as DNA template for HDR instead of AAV6 to target intron 1 *IL2RG*. ssODN was purchased from Integrated DNA Technologies as Ultramer DNA Oligo, designed to maximize HDR efficiency as reported[22] and electroporated at a dose of 200 pmol. Untreated (UT) cells, cells experiencing the sole electroporation (MOCK EL), cells edited with an RNP complex with high specificity (HS) or low specificity (LS), and cells experiencing AAV6 transduction only were employed as controls.

p53 inhibition and anti-inflammatory treatments

CB- or mPB-derived HSPCs were treated with 3.5 μg of p53 inhibitor (GSE56 mRNA) co-electroporated with RNP complex, 50 ng/μL of IL-1 receptor antagonist Anakinra (Kineret, SOBI) and 25 μM InSolutionTM IKK-2 Inhibitor SC514 (Merck, 401485) administered immediately after the GE procedure. All treatments were performed alone or in combination as indicated and negative controls were obtained treating cells with the same volume of DMSO or DPBS vehicle. The GSE56.WPRE construct was cloned from a lentiviral vector expressing GSE56.WPRE[22] into a pVax

plasmid for *in vitro* mRNA transcription containing a T7 promoter, b-globin 30UTR and 64bp-polyA.

Sequences of the gRNAs were designed using an online CRISPR design tool as described in[22] and are reported in Table S1.

Gene editing efficiency analyses

Flow cytometry

Gene editing efficiency was measured from cultured cells *ex vivo* 4 days after electroporation (96h) by flow cytometry, measuring the percentage of cells expressing the GFP marker within HSPC subsets from the more primitive (defined as $CD34^+CD133^+CD90^+$ cells), early progenitors (defined as $CD34^+CD133^+$ cells) and more committed progenitors (defined as $CD34^+CD133^-$). Single-stained, fluorescence-minus-one-stained (FMO), and unstained cells were used as controls. All flow cytometry acquisitions were standardized using SPHERO Rainbow Calibration Particles (8 peaks) (Spherotech, RCP305A). Samples were acquired on FACS Canto II and the collected data were analyzed using the FlowJo software (v. 10.8.1).

Digital droplet PCR (ddPCR)

Genomic DNA was isolated with QIAamp DNA Micro Kit (QIAGEN). 5–20 ng of genomic DNA were analyzed using the QX200 Droplet Digital PCR System (Biorad) according to the manufacturer's instructions. Primers and probes were designed on the junction between the vector sequence and the targeted locus (listed in Table S1). Human TTC5 (Bio-Rad) was used for normalization. Probes for the target were conjugated with FAM, while the TTC5 reference was with HEX fluorophores. Thermal conditions for annealing and extension were adjusted as follows: 95°C × 10 min; 94°C × 30 s, 55°C × 1 min, 72°C × 2 min (40 cycles); 98°C × 10 min. Numbers of edited alleles were calculated with the following formula: (number of AAVS1+ droplets/number of TTC5+ droplets) × 2, as previously described.[9,14,17] Primers and probes are listed in Table S1.

NHEJ analysis

Genomic DNA was isolated with QIAamp DNA Micro Kit (QIAGEN) according to manufacturer's instructions. Nuclease activity (*AAVS1* intron 1, *IL2RG* intron 1) was measured with 5–20 ng of genomic DNA by a PCR-based mismatch-sensitive endonuclease assay amplification of the targeted locus followed by digestion with T7 Endonuclease I (NEB) according to the manufacturer's instructions. Digested DNA fragments were resolved and quantified by capillary electrophoresis on 4200 TapeStation System (Agilent) the manufacturer's instructions. Primers and probes are listed in Table S1.

Colony-forming unit (CFU-C) cell assay

CFU-C assay was performed at the indicated times post-GE for *ex vivo* experiments, at the endpoint (15/18 weeks post-transplantation into NSG mice) for *in vivo* experiments) plating 800 cells (*ex vivo*) or 5000 cells (*in vivo*) in methylcellulose-based medium (MethoCult H4434, StemCell Technologies) supplemented with 100 IU/mL penicillin, 100 μg mL/1 streptomycin. Three (*ex vivo*) or two (*in vivo*) technical replicates were performed for each sample, and the mean value was plotted and used for statistical analysis. Two weeks after plating, colonies were counted, distinguishing erythroid, myeloid, and mixed colonies according to morphological criteria. For large deletion analysis, CFU-C assay was performed at day1 post-GE by plating 400–800 CB HSPCs and 1200 mPB HSPCs in methylcellulose-based medium (MethoCult H4434, StemCell Technologies) supplemented with 100 IU mL−1 penicillin and 100 μg mL−1 streptomycin. Three technical replicates were performed for each condition. Two weeks after plating, single colonies were manually picked for large deletion analysis described below.

Gene expression analysis by RT quantitative PCR (RT q-PCR)

For gene expression analysis, total RNA was extracted using miRNeasy Micro Kit (QIAGEN) according to the manufacturer's instructions, and DNase treatment was performed using RNase-free DNase Set (QIAGEN). 30 ng of cDNA were synthesized with iScript cDNA Synthesis Kit (Bio-Rad). 5ng of cDNA were also pre-amplified using TaqMan PreAmp Master Mix (ThermoFisher) and q-PCR was performed with the Viia7 Real-Time PCR thermal cycler using Fast SYBR Green Master Mix (ThermoFisher), after standard curve method optimization to reach the 100% primer efficiency for each couple of primers listed in Table S1. Three technical replicates were performed for each sample and the relative expression of each target gene was first normalized to *GUSB* housekeeping gene expression and then represented as $2^{-\Delta Ct}$.

$CD34^+$ HSPC xenotransplantation studies in NSG mice

For primary transplantation, $1.5x10^5$ (low dose) or $2x10^5$-$4.5x10^5$ (high dose) CB-derived $CD34^+$ cells or $0.8x10^5$-$3x10^6$ mPB-derived $CD34^+$ cells, diluted in 150 μL of DPBS, were intravenously injected 24h post-GE into 8–10-week-old NSG mice after sublethal irradiation (150–180 cGy). Mice were randomly attributed to each experimental group before injections. Human $CD45^+$ cell engraftment and the presence of gene edited cells (GFP^+ cells by flow cytometry) were monitored by a serial collection of blood from the mouse tail (5/6, 9,12,15/18 weeks post-transplantation) and, at the end of the experiment (6 or 15/18 weeks after transplantation), BM and spleen were harvested and analyzed.

Flow cytometry

Immunophenotypic analyses were performed by flow cytometry using Canto II (BD Pharmingen, BD FACSDiva software) using the antibodies listed in the key resources table. For *ex vivo* analyses, 2-5 × 10^4 cultured cells were analyzed, while for *in vivo* analyses, 2.5 × 10^5-1 x 10^6 mouse-derived cells were analyzed. Cells were incubated with anti-human (*ex vivo*) FcR Blocking (Miltenyi Biotec) or anti-human and anti-mouse FcR Blocking (BD Biosciences) (*in vivo*) before surface marker staining for 10 min at RT. Then, cells were stained for 15 min at 4°C with antibodies listed in the key resources table in a final volume of 50 μL and were washed with DPBS +2% heat-inactivated FBS. Single-stained, fluorescence-minus-one-stained, and unstained cells were used as controls. All flow cytometry acquisitions were standardized using SPHERO Rainbow Calibration Particles (8 peaks) (Spherotech, RCP305A) and the collected data were analyzed using the FlowJo software (v. 10.8.1).

Fluorescent senescence-associated-β-galactosidase staining with SPiDER-β-Gal and CDKN2A (p16) intracellular staining

Senescence-associated-β-Galactosidase (SA-β-Gal) staining was performed with the fluorescent SPiDER-β-Gal system recently developed by Dojindo (SG02-10)[68] used to quantify senescent cells in tissues.[69] Cell suspensions (5-10 x 10^4 cells from *ex vivo* cell culture or of BM-derived $CD34^+$ cells at the endpoint (6w or 15/18 weeks post-transplantation) or cells in 50 μL of peripheral blood collected overtime from NSG mice or 50 μL of total BM retrieved from NSG mice at the endpoint; or colonies plated in semisolid medium were washed with DPBS + 2% heat-inactivated FBS, resuspended in 100μL and treated at 37°C for 1h with Chloroquine (working concentration of 150 μM). SPiDER-β-Gal was added at the final concentration of 0.57 ng/μL to cell suspension at 37°C for 15 min and then washed with DPBS +2% heat-inactivated FBS. Single-stained, fluorescence-minus-one-(FMO) stained, and unstained cells were used as controls. Threshold of positivity was set on fluorescence-minus-one-stained (FMO) or unstained controls. Given the metabolic nature of the assay and sample to sample fluorescence variability, when necessary gating was adjusted to detect cells with a high SPiDER-β-Gal signal.[69] All flow cytometry acquisitions were standardized using SPHERO Rainbow Calibration Particles (8 peaks) (Spherotech, RCP305A).

CellPress
OPEN ACCESS

Intracellular staining for p16 was performed on cell suspensions (5-10 x 10^4 cells from *in vitro* cell culture or of BM-derived $CD34^+$ cells at the endpoint (15/18 weeks post-transplantation) or the equivalent of 1 technical replicate for CFU-C assay) washed with DPBS + 2% heat-inactivated FBS, resuspended in 100μL and fixed with 4% paraformaldehyde (Santa Cruz Biotechnology) at RT for 15 min. Then, cells were washed again with DPBS +2% heat-inactivated FBS and permeabilized with 100 μL of 1X Click-iT saponin-based permeabilization (ThermoFisher) at RT for 30 min. Cells were then incubated overnight at 4°C, in gentle agitation, with anti-p16 primary antibody (Cell Signaling Technology) diluted 1:500 in 1X Click-iT saponin-based permeabilization (ThermoFisher). After an overnight of staining, cells were washed with DPBS +2% heat-inactivated FBS and stained with Donkey anti-Rabbit IgG (H + L) Highly Cross Adsorbed Secondary Antibody, Alexa Fluor 647 (ThermoFisher) for 1h at RT. After washing with DPBS +2% heat-inactivated FBS, samples were acquired. Threshold of positivity was set on isotype and/or secondary antibody controls. Given sample to sample fluorescence variability, when necessary gating was adjusted to detect cells with a high p16 signal. All flow cytometry acquisitions were standardized using SPHERO Rainbow Calibration Particles (8 peaks) (Spherotech, RCP305A).

Samples were acquired on FACS Canto II or FACSymphony A5 SORP (BD FACSDiva software) and the collected data were analyzed using the FlowJo software (v. 10.8.1).

Immunofluorescence analysis

Multitest immunofluorescence slides (15 wells, MP Biomedicals) were treated for 20 min with Poly-L-lysine (already prepared at concentration 100 μg/mL – Sigma Aldrich). After three washes with DPBS 1X solution, approximately 3-5 X 10^4 cells were seeded on covers for 20 min and then fixed with 4% paraformaldehyde (PFA, Santa Cruz Biotechnology) for other additional 20 min. Residual PFA was washed twice with DPBS 1X and cells were permeabilized with 0.1–0.3% Triton X-100 for 10 min at RT, then washed 2–3 times in DPBS 1X and blocked for 30 min with 0.5% BSA and 0.2% fish gelatine in DBPS. After blocking, cells were probed with the indicated primary antibodies diluted in PBG 1X reported concentration in Table S1 for 1 h at RT in a humified chamber, then washed three times with 0.5% BSA and 0.2% fish gelatine in DBPS. After primary antibodies incubation (Anti-53BP1 Antibody, Bethyl Laboratories; Anti-phospho Histone H2A.X (Ser139) Antibody, clone JBW301 (γH2AX); NF-κB p65 (D14E12) XP Rabbit mAb, Cell signaling) cells were washed three times with DPBS and incubated with Alexa 568- and/or 647-labeled secondary antibodies (Invitrogen) (see key resources table) diluted in 0.5% BSA and 0.2% fish gelatine in DPBS for 1 h in a dark humified chamber at RT. After one wash in 0.5% BSA and 0.2% fish gelatine in DPBS and one in DPBS, staining of nuclear DNA with DAPI (Sigma-Aldrich, see Table S1) was performed for 5 min in the dark at RT, and covers were mounted with Aqua-Poly/Mount solution (Polysciences. Inc) on glass slides (Bio-Optica). After an overnight at RT or until the time of acquisition at 4°C, fluorescent images were acquired using a Leica SP5 Confocal microscope. Quantification of micronuclei on DAPI images, 53BP1, γH2AXfoci distribution and NF-kB cellular localization on immunofluorescence images was performed with ImageJ (v2.9).

BAR-seq library preparation

Library preparation for BAR-seq was performed as previously described.[17] Briefly, for BAR-Seq library preparation PCR amplicons for individual samples were generated by nested PCR starting from >50–100 ng of purified gDNA. The first PCR step was performed with GoTaq G2 DNA Polymerase (Promega) according to the manufacturer's instructions using the following amplification protocol: 95°C for 5 min, (95°C for 0.5 min, 60°C for 0.5 min, 72°C for 0.5 min) × 20 cycles, 72°C for 5 min. Forward primer was designed to bind the donor template upstream of the BAR sequence, while the reverse primer annealed outside the homology arm, thus amplifying 328 bp of the on-target integrated cassette. For targeted deep sequencing of the plasmid and AAV libraries, the reverse primer was annealed to the homology arm. The second PCR step was performed with GoTaq G2 DNA Polymerase (Promega) according to the manufacturer's instructions using 5 μL of the first-step PCR product and the following amplification protocol: 95°C for 5 min, (95°C for 0.5 min, 60°C for 0.5 min, 72°C for 0.5 min) × 20 cycles, 72°C for 5 min. Second-step PCR primers were endowed with tails containing P5/P7 sequences, i5/i7 1000 Illumina tags to allow multiplexed sequencing, and R1/R2 primer binding sites. PCR amplicons were separately purified using the MinElute PCR Purification kit (QIAGEN). Concentration and quality of amplicons were assessed by using a QuantiFluor ONE dsDNA system and a 4200 Tapestation system (Agilent Technologies). Amplicons were then multiplexed and run by the San Raffaele COSR on MiSeq 2 × 75 bp or 2 × 150 bp (Illumina).

BAR-seq analyses

BAR-seq data were with the BAR-Seq2 pipeline (available at https://bitbucket.org/bereste/bar-seq2). In detail, input reads were preprocessed to trim low-quality bases and keeping sequences having length ≥75bp (options: -m 75 -q 30) to ensure the proper amplicon structure within each read. Barcode sequences (BARs) were then extracted using TagDust (v.2.33)[70] and corrected using a community-based strategy on a graph built on the sequence similarity (edit distance ≤2). The resulting barcodes were quantified based on their abundance (number of supporting reads) and filtered, keeping only those having a minimum count equal to 2. Finally, dominant clones were identified by ranking the computed barcodes based on their abundance and cutting the resulting distribution at the elbow point.

Indels-based clonal tracking library preparation

Library preparation for Indels-based clonal tracking was performed as previously described.[17] PCR amplicons for individual samples were generated by nested PCR starting from >50–100 ng of purified gDNA. The first PCR step was performed with GoTaq G2 DNA

Polymerase 1007 (Promega) according to the manufacturer's instructions using the following amplification protocol: 95°C for 5 min, (95°C for 0.5 min, 60°C for 0.5 min, 72°C for 0.25 min) × 20 cycles, 72°C for 5 min. The second PCR step was performed with GoTaq G2 DNA Polymerase (Promega) according to manufacturer's instructions using 5 μL of the first-step PCR product and the following amplification protocol: 95°C for 5min; 95°C × 0.5 min, 60°C × 0.5 min, 72°C × 0.3 min, (20cycles); 72°C × 5 min. Second-step PCR primers were endowed with tails containing P5/P7 sequences, i5/i7 Illumina tags to allow multiplexed sequencing and R1/R2 primer binding sites. The PCR amplicon from each sample was separately purified by using a QIAquick PCR Purification kit (Qiagen). Concentration and quality of amplicons were assessed by using a QuantiFluor ONE dsDNA system and 4200 Tapestation system (Agilent). Amplicons from up to 49 differently tagged samples were multiplexed at equimolar ratios and run by the San Raffaele Center for Omic Sciences (COSR) using 2 × 300 bp paired-end MiSeq 600 (Illumina).

Indels-based clonal tracking analysis

Samples for indels-based clonal tracking were analyzed with CRISPResso2 (v2.2.8)[65], to detect and quantify the small variants in reads from editing experiments (e.g., insertions, mutations, and deletions). In detail, for each sample, input reads were pre-processed (CRISPResso2 options: –trim_sequences –trimmomatic_command trimmomatic –

trimmomatic_options_string 'ILLUMINACLIP: TruSeq3-PE-2.fa:2:30:10 MINLEN:100′) to get rid of low-quality positions (score <30) and to remove Illumina adapters, keeping only trimmed sequences longer than 100 bp to ensure the full coverage of the region of interest.

Then, sequences were mapped to the input amplicon reference and the quantification window was set to 1bp around the cut site, identified by exploiting the provided sgRNA sequence. Computed alleles were quantified by measuring the number of reads and their relative abundance based on total read counts. Finally, CRISPResso2 output alleles were post-processed by correcting all the mismatch

positions outside the quantification window and re-quantifying the total read counts and consequently the corresponding relative abundances, filtering out those having a relative abundance lower than the false positive threshold positive threshold (set at 0.2%, based on untreated controls).

Total RNA-Seq library preparation

Whole transcriptomic analysis was performed on a pool of CB-derived HSPCs. All conditions were performed in triplicate. Total RNA was isolated using miRNeasy Micro Kit (QIAGEN), and DNAse treatment was performed using RNase-free DNAse Set (QIAGEN), according to the manufacturer's instructions. RNA was quantified with The Qubit 2.0 Fluorometer (ThermoFisher) and its quality was assessed by a 2100 Agilent Bioanalyser (Agilent Technologies). Minimum quality was defined as an RNA integrity number (RIN) of >8. 300 ng of total RNA was used for library preparation with strand-specific RNA-seq with PolyA selection kit (Illumina) for the RNA-seq in Figure 1 at day 1, TruSeq Stranded mRNA (Illumina) for the RNA-seq in Figure 4 at day 1 (paired-end), SMART-seq Ultra Low Input unstranded for RNA-seq in Figure 4 at day 4 (single-end). Samples were sequenced by the San Raffaele COSR or Genewiz (Azenta Life Sciences) using a NextSeq 500 High 75 (Illumina) or NoveSeq 2 x 150 bp sequencing configuration to obtain 10-30 x 10^6 reads per sample.

Bulk and single-cell RNA-seq analyses

For RNA-seq analysis, sequenced reads were inspected for quality, trimming the adapter sequences with Trim Galore (https://www.bioinformatics.babraham.ac.uk/projects/trim_galore/). Filtered reads were aligned to the human genome (GENCODE GRCh38 primary assembly) with STAR release 2.7.6a.[71–73] The quantification of gene expression was obtained with featureCounts v2.0.1 (Liao, Smyth, and Shi, 2014), with the following parameters (reverse paired-end for data generated at day 1 post-GE, unstranded single-end for day 4 post-GE) and using the annotation GTF file from GENCODE (version v35 primary assembly). Quantified reads were normalized by library size, and the differential expression (DE) analysis was performed with the DESeq2 package (Love, Huber, and Anders, 2014), retaining significant genes upon *p*-value correction with the Benjamini-Hochberg method (FDR <0.05). For the Gene Set Enrichment Analysis (GSEA) all genes were ranked by decreasing Log_2FC values. The analysis was performed considering the Hallmark signatures from the MSigDB database[64] and gene signatures regarding the senescence program from literature.[34–37,69,74–76] The published scRNA-seq dataset GEO: GSE119597,[14] was interrogated to evaluate the expression levels of senescence-associated gene signatures from literature[38,74] with the AddModuleScore function from the Seurat package. The signature average expression level for each cell was plotted with the function VlnPlot for each condition and cluster. The statistical differences between conditions were computed with Pairwise Wilcoxon Rank Sum Tests, reporting the *p*-value adjusted by Benjamini–Hochberg procedure.

Analysis of large deletions at the edited site

Two weeks after plating, single colonies were manually picked for large deletion mutational analysis. gDNA was isolated with QuickExtract DNA Extraction Solution (Lucigen) from single colonies according to the manufacturer's instructions. For large deletion droplet digital PCR (ddPCR) analyses, 5–50 ng of gDNA from single colonies was analyzed using the QX200 Droplet Digital PCR System (Bio-Rad) according to the manufacturer's instructions. Commercial probes used are listed in Table S1. Thermal conditions for long-range deletions were adjusted as follows: 95°C x 10′min, (94°C × 0.5 min, 60°C × 1 min) x 40 cycles, 98°C × 10 min. Human

TTC5 (Bio- Rad) assay was used for normalization. Deletion analysis was calculated with the following formula: (number of AAVS1+ droplets/number of normalizer TTC5+ droplets) × 2.

Translocation analysis on colonies derived from HSPCs

For chromosome X-14 (chrX-chr14) translocation involving *IL2RG* locus, ddPCR, primers, and probes were designed on the junction between the two RNP cleavage sites on both chromosomes and control sequences used for normalization (human TTC5 genes) and are listed in Table S1. Thermal conditions for annealing and extension were: 55°C for 30 s, 72°C for 2 min.

CAST-seq

Genomic DNA was extracted using the DNeasy Blood & Tissue kit (Qiagen) according to the manufacturer's protocol and with the addition of RNase treatment (Qiagen). Primer sequences used for CAST-Seq are listed in Table S1. CAST-Seq analyses were performed as originally described,[45] with few modifications.[77,78] In brief, 500 ng of genomic DNA were used as input material for each technical replicate. Libraries were prepared using the NEBNext® Ultra™ II FS DNA Library Prep Kit for Illumina (NEB E7805L). Enzymatic fragmentation of the genomic DNA was aimed at an average length of 500–700 bp. CAST-Seq libraries were sequenced on a NextSeq6000 using 2x150 bp paired-end sequencing (GENEWIZ, Azenta Life Sciences). For each sample, two biological replicates were run and analyzed. Only sites that were present in both biological replicates and significant in at least one replicate are reported (Table S3). For sites under investigation, the spacer sequence of the gRNA was aligned to the most covered regions for each site (±400 bp).[77] Sites were labeled as OMT if any of the two *p*-values reached the cutoff of 0.005.[78] The presence of large (>200 bp) aberrations (deletions and inversions) was calculated as a percentage of the total on-target reads. Calculations were based on the read coverage in a ±10 kB window around the on-target site, with only the first base located closest to the on-target site of each read included in the computation. The percentage of large aberrations is equal to the sum of all reads with a start position >200 bp from the cleavage site divided by the sum of all reads at the on-target site (Table S2). Note that this value is relative to all CAST-Seq reads at the on-target site, and is not an absolute quantification of on-target aberrations. In Figure 7A, circos plots summarize CAST-Seq analysis of the CRISPR-Cas9 targeting of the *IL2RG* locus in the indicated conditions. In green is reported the on-target site cluster on chromosome X, while in red the off-target on chromosome 14. From the outer to the inner layer a red ring indicates the alignment score against the gRNA sequence, with significant score accentuated by red dots; and a blue ring indicates the length of sequence homology, with significant lengths emphasized by blue dots. Arcs highlight the identified translocations between on-target site and the off-target site.

Whole exome sequencing sample preparation and analysis

CB-derived HSPCs across editing conditions were collected 7 days after the procedure to perform 500X Whole Exome Sequencing (WES) analysis of the *ex vivo* bulk population. The same HSPCs were infused one day post-GE in NSG mice, and live human $CD45^+$ cells from BM were retrieved 15 weeks after infusion for 500X WES. WES was performed by Genewiz (Azenta) using the Agilent SureSelect Human All Exon V7 kit and running an Illumina NovaSeq 2x150bp with an estimated output of ~50Gb (500X) per sample and analyzed following the GATK "Best Practice Workflows" to identify variants in each sample. In details, input reads were pre-processed with FastQC (v0.11.9) to assess their quality and trimmed using trim-galore (v0.6.6) to get rid of low-quality bases. Moreover, to remove possible mouse contaminations due to the cell transplant procedure, a disambiguation procedure was performed[79]: reads were aligned on both human and mouse reference genomes, and then each one was assigned to the organism having the best mapping (or marked as ambiguous and discarded). Next, all samples were randomly downsampled to 75M reads using the Seqtk toolkit (v1.3) to avoid sample unbalance, and the reads were then aligned to the human genome assembly (GRCh38) using the BWA (v0.7.17). Alignments were processed to mark duplicates using Picard (v2.25.6) MarkDuplicates, and GATK (v4.2.0.0) BaseRecalibrator + ApplyBQSR were used to recalibrate base quality scores on dbSNP known sites. HaplotypeCaller in GVCF mode was used to call variants in each sample, which were then combined using CombineGVCFs and genotyped with GenotypeGVCFs. Resulting variants were filtered using VariantFiltration based on their 'QualityByDepth' (i.e., –filter-expression 'QD < 2.0') and overall coverage 'DP' (i.e., –filter-expression 'DP < 500'). To identify private variants belonging to each sample additional filters were applied, i.e., variants having low genotype quality (i.e., GQ < 80) and low coverage (i.e., DP < 50) were removed. Variants were then annotated with SnpSift (v5.0) on the dbSNP database. Vitro samples for each condition were used as germline reference, and variants appearing in 50% of those samples (at least 4 out of 8) were filtered out from all other samples, as they were considered as present in the initial cell population and not induced by treatments. As a further refinement, multi-allelic variants (mainly involving repetitive sequences) and those belonging to non-canonical chromosomes were not considered for the analysis. The resulting variants were annotated using SnpEff (v5.0) on the canonical isoform from the GRCh38.p13.RefSeq reference database. Downstream analysis of the final variants was done by classifying them based on their type (insertion, deletion, or SNV), and focusing on all SNV to classify mutation events.

Assessment of variants using a panel of cancer as well as on clonal hematopoiesis related genes (Tables S3 and S4) was performed based on variant annotations. Having observed that the number of identified variants is associated with the initial library complexity, which in turn is negatively influenced by the number of PCR cycles used during library preparation, we have constructed a mixed linear model to account for the different number of PCR cycles used. The model was build using the "lme4" R package with the following formula: lmer(Number of Variants ~ 2^PCRCycle + (1 | Group)). This model was then used to predict the expected number

of variants based on the number of PCR cycles used for library preparation in each sample. Finally, to account for potential read coverage bias, we normalized the number of predicted variants against the number of callable nucleotides. Callable nucleotides were defined as those with a coverage of at least 50X and were determined using Samtools (v1.7) depth by counting the number of nucleotides with a coverage $\geq$50.

QUANTIFICATION AND STATISTICAL ANALYSIS

The number of biologically independent samples, animals, or experiments is indicated by n. For some experiments, different HSPC donors were pooled to account for donor-related variability and to reach the number of cells needed for the analyses. Data were summarized as median or mean ± SEM depending on data distribution. Inferential techniques were applied in the presence of adequate sample sizes ($n \geq 3$); otherwise, only descriptive statistics are reported. The Mann–Whitney test was performed to compare two independent groups, while in the presence of more than two independent groups, the Kruskal–Wallis test was used. The Wilcoxon test and Friedman test were then applied for repeated measures design. Spearman's correlation coefficient was calculated to evaluate the presence of a monotonic relationship between variables. Data characterized by complex forms of dependency among observations were analyzed using random-intercept Linear Mixed-Effects models (LMEs), specifying random-effect terms, including nested effects when necessary, on both experimental units and experiment ID codes to better capture underlying structure and data heterogeneity. This LME approach was also applied to time-course data, with treatment group, time, and their interaction included in the model as fixed effects, while random effects were specified similarly to account for dependencies and variability across observations.

When fitting LME models, standard transformations (logarithm, square/cubic root and ordered quantile normalization) were applied to outcome variables to satisfy model assumptions. Post hoc analysis after LME was performed to evaluate pairwise comparisons of interest, fixing other variables included in the model at a chosen value. Bonferroni's approach was used as method to adjust *p*-values for multiple comparisons. Analyses were performed using GraphPad Prism software v.10.0.2 (GraphPad) and R statistical software (version 4.4.1; https://cran.r-project.org/index.html). Differences were considered statistically significant at $^{*}p < 0.05$, $^{**}p < 0.01$, $^{***}p < 0.001$, $^{****}p < 0.0001$, and "ns" stands for not significant. Values were indicated when comparisons were approaching significance with p value <0.08.